Materials Today Bio 37 (2026) 102872

Contents lists available at ScienceDirect

Materials Today Bio

journal homepage: www.journals.elsevier.com/materials-today-bio

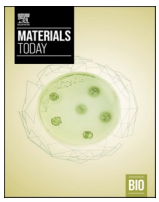

A paradigm shift from penetration: Material-based solutions for multidimensional spatiotemporal, hypoxic, and optical challenges in cutaneous photodynamic therapy

Xun Feng [a,1], Hua Fan [c,1], Lubin Zhou [d,1], Zhilong Zhao [c], Mu Yang [c,*], Xinxing Sun [d,**], Yang Chen [b,***]

[a] Department of Sanitary Chemistry, School of Public Health, Shenyang Medical College, Shenyang, 110034, China
[b] Department of Pharmaceutics, School of Pharmacy, China Medical University, Shenyang, 110122, China
[c] Liaoning Inspection Examination & Certification Centre, Liaoning Provincial Institute for Drug Inspection and Testing, Shenyang, 110031, China
[d] Wenzhou Institute, Institute of Translational Medicine, Shanghai University, Shanghai, 200444, China

ARTICLE INFO

Keywords:
Photodynamic therapy
Smart material
Photosensitizer
Cutaneous drug delivery
Microneedle
Nanozyme

ABSTRACT

Despite considerable advancements in pharmaceutical strategies (e.g., nanocarriers, physical enhancement) to overcome the skin barrier for topical photodynamic therapy (PDT), clinical translation remains impeded by unresolved challenges. While previous reviews have predominantly focused on enhancing photosensitizer permeation, this work shifts the paradigm to systematically address three critical yet under-reviewed barriers: insufficient spatiotemporal precision in photosensitizer delivery, hypoxia-induced therapeutic resistance, and inefficient photon utilization. This review critically evaluated the transformative evolution from conventional formulations toward "smart" therapeutic architectures, presenting a coherent framework of material-based solutions engineered to overcome these specific challenges: (1) depth-resolved, stimuli-responsive, and molecular-targeted release mechanisms; (2) transdermal oxygen self-replenishing systems (e.g., catalase-mimetic nanomaterials or perfluorocarbon-based reservoirs); and (3) synergistic optical components to enhance photon utilization, including tissue optical clearing agents, light-guiding channels, and multifunctional light-responsive platforms. These integrated strategies enable the dynamic synchronization of photosensitizer bioavailability with pathological microenvironmental demands, allowing precise modulation across spatial, temporal, and dosage dimensions. Furthermore, we incorporated an analysis of commercially available and clinically investigated photosensitizers, providing critical context for the current state and future trajectory of the field. By bridging interdisciplinary insights from materials science, drug delivery, and photobiology, this work outlines a transformative roadmap for next-generation, precision-based dermatological therapies, marking a clear departure from penetration-centric approaches.

1. Introduction

Photodynamic therapy (PDT) is a clinically validated photochemical treatment modality that operates via light-activated photosensitizers (PSs), which produce reactive oxygen species (ROS) to exert cytotoxic effects on targeted tissues [1,2]. Through effective PDT, multifactorial therapeutic effects can be achieved, including effectively facilitating the eradication of neoplastic cells, inactivation of microbial pathogens, disruption of vascular networks, and modulation of immune responses [3,4]. Given the easy accessibility of skin to PSs and light, topical PDT is particularly preferred for treatment of both malignant and nonmalignant cutaneous diseases [5].

Current clinical guidelines, supported by robust evidence, strongly recommend PDT for the management of actinic keratosis, superficial cutaneous malignancies (such as Bowen's disease and superficial basal cell carcinoma), reversal of photoaging, treatment of acne vulgaris,

* Corresponding author.
** Corresponding author.
*** Corresponding author.
E-mail addresses: 277754599@qq.com (M. Yang), xinxingsun6820@163.com (X. Sun), chenyangpharm@163.com, yangchen@cmu.edu.cn (Y. Chen).
[1] Contribute equally to this work.

https://doi.org/10.1016/j.mtbio.2026.102872
Received 5 December 2025; Received in revised form 17 January 2026; Accepted 28 January 2026
Available online 29 January 2026

recalcitrant verrucae, cutaneous leishmaniasis, and onychomycosis [6]. PSs are generally administered externally to the skin, which enables direct access to the targeted organ of topical PDT and avoids their systemic phototoxicity [7]. The therapeutic efficacy primarily depends on photophysical processes involving PSs excitation: upon light absorption, ground-state PSs molecules undergo intersystem crossing to excited triplet states, subsequently initiating oxygen-dependent ROS generation through either electron transfer (Type I reaction) or energy transfer (Type II reaction) pathways [2,8]. Of these, the Type II mechanism involving singlet oxygen ($^1O_2$) production predominates in clinical PDT applications due to its superior cytotoxic potential, though its oxygen-dependent nature imposes inherent limitations in hypoxic tumor microenvironments [9].

Despite two decades of clinical implementation, significant translational challenges persist that constrain PDT optimization [10,11]. While existing reviews have predominantly focused on enhancing skin penetration of PSs [12,13], critical limitations beyond permeability including imperfect spatiotemporal control of PSs activation, hypoxia-induced therapeutic resistance, suboptimal light penetration and utilization efficiency, and formulation-dependent PSs instability remain systematically underexplored. Key limitations include imperfect spatiotemporal control of PSs activation, hypoxia-induced therapeutic resistance, suboptimal light penetration and utilization efficiency, and formulation-dependent PSs instability. To address these interconnected barriers, this review systematically examines recent advances at the convergence of materials engineering, targeted drug delivery systems, and optical innovation. In accordance, this review would provide a systematic dissection of these multidimensional barriers hindering the clinical translation of topical PDT, and propose critical solutions that integrate material science, intelligent drug delivery, and optical engineering (Fig. 1). The paper uniquely maps the technological evolution from conventional formulations to next generation "smart" therapeutic architectures, highlighting their potential to synchronize PSs bioavailability with dynamic microenvironmental demands.

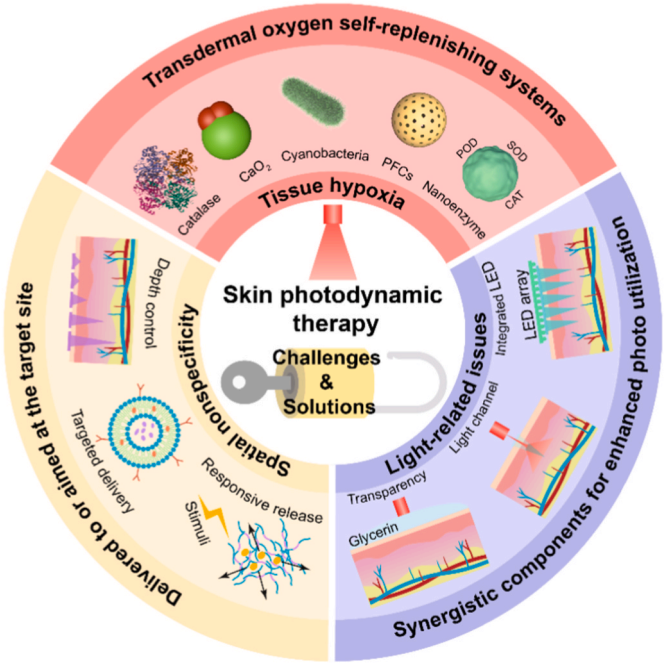

Fig. 1. Challenges in cutaneous PDT and innovative strategies.

2. Spatiotemporal constraints of the PSs and material-based strategies

2.1. Spatiotemporal constraints

Conventional topical formulations usually exhibit poor spatial selectivity because of the passive diffusion mechanisms. The transportation of PSs in the skin follows two distinct spatial trajectories: lateral diffusion within the stratum corneum and adjacent epidermis, and vertical permeation through the dermal-epidermal junction into systemic circulation [14]. This spatial dichotomy poses dual risks. The lateral dispersion facilitates PSs accumulation in perilesional healthy tissues, where unintended light exposure triggers localized phototoxicity (erythema, edema, desquamation, and hyperpigmentation). Conversely, vertical permeation enables systemic PSs absorption, risking hepatic sequestration and distant organ photosensitization, particularly in sun-exposed regions [15,16].

The contribution of lateral spread and vertical permeation of a PS is governed by both the skin microenvironment and its physicochemical properties [14]. The surface of the skin is covered with a unique blend of lipids (ceramide, cholesterol, and fatty acids) derived from the intercellular space of the stratum corneum or secreted from sebum lipids [17]. Below the stratum corneum are viable epidermis, dermis, and hypodermis, all of which are composed of about 90 % water and thus greatly hydrophilic [18]. For highly lipophilic compounds, they demonstrate preferential epidermal sequestration due to stratum corneum partitioning effects, subsequently manifesting centrifugal diffusion kinetics through intercorneocyte lipid matrix remodeling. By contrast, moderately lipophilic compounds preferentially undergo longitudinal diffusion, generating obconical concentration gradients [19]. Although the lateral lipid diffusion may show no dependence on molecular weight, its contribution to the total drug penetration would be significant for larger molecules [20]. Hydrophilic compounds demonstrate limited stratum corneum permeability due to their poor partitioning with the intercellular lipid matrix; however, their transdermal delivery can be significantly enhanced by co-administration with chemical penetration enhancers or utilization of transappendageal routes. Upon breaching the epidermal barrier, they display accelerated systemic absorption through enhanced capillary network accessibility, particularly under conditions of compromised skin barrier integrity [20–22].

As systematically categorized in Table 1, PSs molecules can be categorized into distinct families based on their inherent structural motifs and features, generally including porphyrins, porphyrin precursors, chlorins, phthalocyanines, natural sensitizers, and fluorescent dyes. These structural variations critically govern their physicochemical profiles, particularly molecular weight (*MW*) and logarithm of the octanol-water partition coefficient (*log Ko/w*, commonly abbreviated as log *P*), both of which collectively determine their skin penetration patterns. Theoretical mathematical models (QSAR) can predict that PSs with varying *MW* and log *P* would have different tendencies to systemic absorption (governed by transdermal permeation coefficients, K_p) or lateral diffusion (dependent on stratum corneum lipid fluidity, Klateral). Hydrophobic agents (log $P > 3$) preferentially undergo centrifugal dispersion through intercorneocyte lipid lamellae, whereas hydrophilic counterparts (log $P < 0$) favor vertical permeation into capillary networks.

In addition, conventional PSs molecules, lacking intrinsic molecular recognition capabilities, often fail to achieve precise spatiotemporal targeting, resulting in suboptimal therapeutic outcomes. For those diseases (e.g., acne vulgaris) originating from cutaneous appendages, the absence of appendage-targeting mechanisms would also result in inefficient appendage penetration and non-specific activation consequences. Therefore, the non-specific permeation of PSs molecules necessitates tailored formulation strategies to optimize their target-site accumulation while minimizing off-target effects.

Table 1
The commonly used PSs and their physicochemical properties.

Type	Name	*MW*	Log *P*	Log K_{P1} (transdermal, cm/s)[a]	Log K_{P2} (transdermal, cm/s)[b]	Log K_P (lateral, cm/s)[c]
Porphyrins	Porfimer sodium	1179.36	2.8	−7.93	−7.56	−8.65
	Verteporfin	1437.59	2.1	−10.00	−9.46	−8.77
	Hemoporfin	598.7	2.74	−4.43	−4.34	−8.66
Porphyrin precursors	5-aminolevulinic acid ALA)	131.12	−1.5	−4.58	−4.52	/
	Methyl ALA	145.16	−1.2	−4.46	−4.40	/
Chlorins	Chlorin e6 (Ce6)	596.67	1.2	−5.51	−5.35	−9.02
Natural sensitizers	Curcumin	368.38	3.62	−2.40	−2.47	−8.54
	Hypericin	504.44	3.92	−3.01	−3.04	−8.50
	Resveratrol	228.24	2.57	−2.29	−2.38	−8.69
Fluorescent dyes	Methylene blue	319.85	3.61	−2.11	−2.21	−8.54
	Indocyanine green	774.97	6.05	−3.15	−3.15	−8.32
	Rhodamine B	479.02	1.34	−4.69	−4.60	−8.97

Note for this table.
[a] Calculated according to the empirical equation (Potts and Guy): $\log K_p = -2.72 + 0.71\log P$ - 0.0061 MW.
[b] Calculated according to the empirical equation (US-EPA): $\log K_p = -2.80 + 0.66\log P$ - 0.0056 MW.
[c] Calculated according to the empirical equation: $\log K_p = 0.7\log P$ - 9.09691.

2.2. Material-based strategies

The effectiveness of skin PDT relies on a meticulously designed system that addresses three primary delivery challenges: restricted vertical penetration, unintended activation, and inadequate lesion-specific accumulation. This section explores microneedles (MNs) mediated deep tissue delivery, disease-responsive material platforms, and molecular recognition strategies. These approaches collectively facilitate anatomical precision, pathologically triggered activation, and subcellular targeting, thereby transitioning PDT from passive diffusion to active interaction with the local microenvironment.

2.2.1. MNs mediate depth-resolved delivery in the skin

MN arrays are micron-sized projections that enable spatially controlled transdermal delivery through minimally invasive microchannel creation, bypassing the stratum corneum barrier to achieve localized drug deposition within specific skin strata (epidermis, dermis, or hypodermis). They can be fabricated from diverse materials including stainless steel, silicon, and biomacromolecules (e.g., hyaluronic acid), and engineered into structurally distinct forms such as solid, coated, hollow, or dissolvable configurations for meeting different delivery demands [23].

Generally, the human skin is anatomically organized into three layers, progressing from superficial to deep: the stratum corneum (a keratinized barrier layer, 10–20 μm), the viable epidermis (hosting active metabolic activity, 50–100 μm), and the dermis (providing structural support through collagen and elastin networks, 1–2 mm) [24]. Therefore, the length of MNs is a critical design parameter that can be elaborately modulated for layer-specific delivery in the skin. Generally, they require a minimum length of 20 μm to effectively penetrate the stratum corneum for epidermal delivery and 150 μm to traverse the viable epidermis and reach the dermis. In addition, it should be noted that the penetration depth can also be affected by other factors, such as the insertion force and the structural features of the MNs [25].

Tip-loaded dissolving MNs are the preferred design for layer-specific drug delivery due to their unique layered architecture. The drug-loaded tip layer confines therapeutic agents (e.g., PSs) to the needle apex, ensuring localized release within the targeted skin region, while the rest layer provides mechanical robustness during insertion while rapidly dissolving post-application to minimize residual material [26,27]. This stratified design enables depth-resolved control of drug release, making it ideal for PDT applications requiring precise PSs activation.

In conventional tip-loaded MNs, drug payloads (e.g., PSs) can be loaded throughout the entire needle body with a non-therapeutic backing layer, which significantly reduces superficial drug diffusion and retention in the upper epidermis. For example, Zhao et al. developed such a sodium hyaluronate MN patch containing 122 μg ALA mainly distributed in the tips with a height of 907 ± 20 μm (Fig. 2a). After treatment of the skin for 2 min, the MNs could effectively pierce the skin and achieve an insertion depth of 218 ± 52 μm (Fig. 2b–d), which was shorter than the MN height, probably due to the presence of skin elasticity and the rapid dissolution of the MN. This insertion capacity enables the MNs to pierce through the stratum corneum and reach the dermis layer, facilitating their PDT efficacy against subcutaneous tumor (97 % inhibition rate versus 66 % in the injection group) (Fig. 2e–h) [28]. Similarly, He et al. engineered a comparable MN system to achieve the localized delivery of 5-ALA and enhance the intratumoral accumulation of protoporphyrin IX, namely the photosensitive metabolite derived from 5-ALA [30].

Modern advancements pioneer apex-specific drug loading, where only the needle tip contains the active compound, while the remaining shaft and backing layer are fabricated from identical or different matrix materials (e.g., hyaluronic acid, PVP). This structural refinement enhances vertical penetration precision, enabling targeted delivery to deeper dermal layers. With sodium hyaluronate and polyvinyl alcohol as the matrix in different sections, an MN array consisting of a hemoporfin-loaded apex (140 μm) and a transparent needle shaft (660 μm) was fabricated (Fig. 2i and j). The transparency of the needle body facilitated the light penetrating through the MN (Fig. 2k). After insertion into the skin, the HA tips could fully dissolve within 5 min (Fig. 2l–q). At a high insertion ratio, the MNs achieved a relatively narrow distribution of the payload in the skin, starting from 40 μm to 180 μm (Fig. 2r–t). This optimization enhances the utilization rate of PS, and its dosage was reduced to 0.17 % of the amount used in the clinical method [29].

However, it should be noted that upon dissolution of the MN matrix, the released drug relies entirely on passive diffusion governed by concentration gradients, with no active mechanism to regulate spatiotemporal distribution or penetration depth. This lack of post-dissolution control would also compromise their efficacy in targeting deep-seated lesions or confining drug action to specific microenvironments, often resulting in off-target effects and suboptimal bioavailability. Consequently, the current dissolvable MNs remain inadequate for precision therapies requiring dynamic control over drug migration, which is a challenge driving the development of next-generation systems incorporating stimuli-responsive materials, actively targeted molecules, or external guidance modalities (e.g., magnetic fields, ultrasound) to steer drug behavior post-administration [31].

2.2.2. Stimuli-activatable functional materials enable on-demand release at pathological sites beneath the skin

Stimuli-activatable platforms significantly improve the localized precision of PDT by restricting PSs activation to pathological microenvironments, thereby minimizing off-target phototoxicity. These smart carriers exploit disease-specific endogenous cues (e.g., acidic pH,

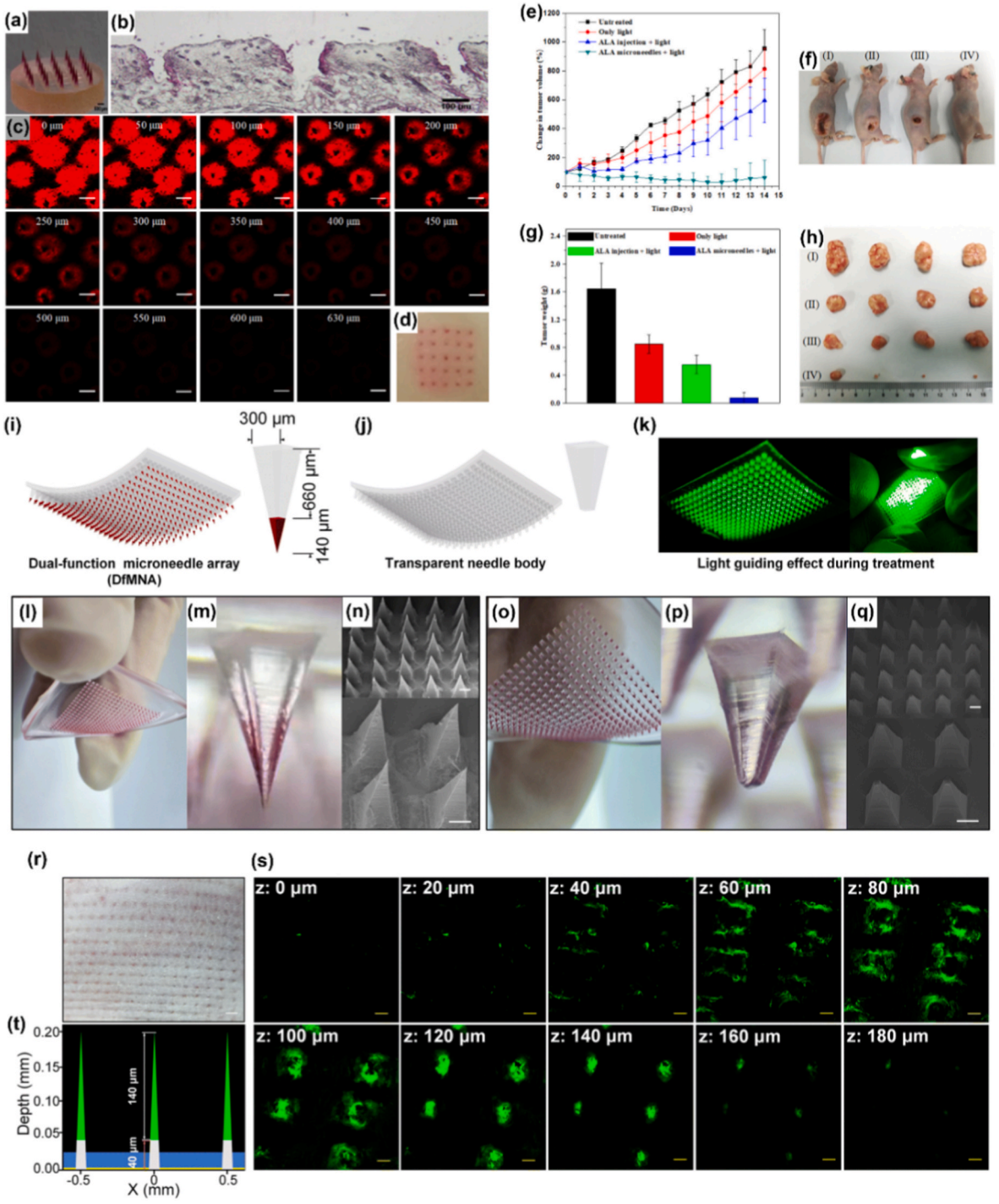

Fig. 2. Tip-loaded MNs (a–h) and apex-loaded MNs (i–s) for depth-resolved delivery in the skin, including (a) stereomicroscopy image of the conventional tip-loaded MNs, (b) histological section of the mouse skin treated by MNs, (c) CLSM images of the mouse skin after insertion of the rhodamine 6G loaded MNs for 2 min, (d) bright-field micrograph of the treated skin, (e) tumor growth curves tumor-bearing mice after PDT by the ALA-loaded MNs, (f) representative images of tumor-bearing mice after 14 days' treatment, (g) weight of excised tumor, (h) images of excised tumor, (i) schematic illustration of the apex-loaded MNs, (j) schematic illustration of the transparent needle body, (k) the light guiding effect of the MNs illuminated by 525 nm green light, (l) photo of the apex-loaded MNs, (m) photo of a single MN, (n) SEM of the MNs (scale bar: 200 μm), (o) photo of the MNs after the tips dissolved, (p) photo of a single transparent needle body, (q) SEM of the MN after the tips dissolved (scale bar: 200 μm), (r) bright field image of the mouse skin after insertion of the MNs, (s) CLSM images of the skin from the skin surface (0 μm) to 180 μm beneath the skin (scale bar: 100 μm), (t) scheme of needle insertion. Copied with permission [28,29]. Copyright 2018, Elsevier. Copyright 2022, RSC.

hypoxia, elevated ROS/H_2O_2 levels, or overexpressed enzymes) or externally applied triggers (light, heat, magnetic fields) to transition from a quiescent state ("off") during delivery process to an activated state ("on") at target lesions. Upon stimulus exposure, they undergo structural/chemical transformations (e.g., bond cleavage, phase transitions) to release PSs and generate cytotoxic ROS in situ, enhancing the selectivity and accuracy of PDT [32–34].

For endogenous stimuli-responsive strategies, PSs can be engineered

as prodrug-based precursors or assembled into stimuli-labile nanocarriers. These systems remain pharmacologically inert until encountering diseased microenvironmental cues, such as acidic pH or elevated H_2O_2/ROS/enzymes, triggering the pro-photosensitizer or PS-loaded carrier degradation via responsively cleavable bonds or linkers [35–37]. This spatiotemporally precise activation ensures localized release of active PSs, minimizing off-targeted phototoxicity while enhancing intralesional ROS generation. For instance, a hydrophilic protophorphyrin IX (PpIX) derivative conjugated to the adipic dihydrazide (ADH) functionalized hyaluronic acid (HA) was introduced into a tumor acidic microenvironment activatable dissolving MN via the crosslinking its hydrazide bond to the aldehyde group of protocatechualdehyde-Fe^{3+} complex to form the matrix material with pH sensitive acylhydrazone bond. With the pH decreased from 7.4 to 5.0, the drug release rate was dramatically increased, ensuring an enhanced chemo-PDT towards melanoma [38]. Since MNs enable direct cellular delivery of therapeutic payloads, other stimuli-responsive nanocarriers or PS prodrugs, originally engineered for injectable systems, can be synergistically integrated with MN platforms to achieve spatiotemporal control over PDT activation. These responsive strategies (e.g., enzyme-cleavable coatings, hypoxia-responsive nanocarriers) have been systematically reviewed elsewhere, with recent advances demonstrating enhanced specificity and reduced off-target phototoxicity in preclinical models [32,36].

External stimuli (e.g., light, magnetic fields, or ultrasound) would also enable spatiotemporally precise localization of PSs to targeted skin regions (e.g., dermal or subcutaneous tumors) [39]. For instance, a magnetic nanocomposite film based on bacterial cellulose was engineered as a stimuli-responsive platform for enhanced transdermal PDT and chemotherapy. This system integrates superparamagnetic Fe_3O_4 nanoparticles co-loaded with the PS hematoporphyrin monomethyl ether and chemotherapeutic doxorubicin. Surface modification with folic acid (FA) conferred active tumor-targeting capability by binding to overexpressed folate receptors on breast cancer cells. Under external magnetic guidance, the nanocomposite achieved deep-seated lesion targeted delivery and achieved breast cancer treatment [40].

The stimulus-responsive strategies successfully implemented in other therapeutic areas can be directly adapted to innovate the cutaneous PS delivery systems. Notable examples include the glucose-sensitive insulin patches pioneered by Gu' group [41,42] and the wound-responsive smart dressing developed by Shen' group [43,44]. Their underlying material-design concepts offer a valuable framework for enhancing PS delivery. For instance, the closed-loop co-delivery platform for insulin and glucogon provides a paradigmatic inspiration for self-optimizing both drug availability and therapeutic microenvironment via the simultaneous release of a PS and a complementary modulator in response to real-time microenvironment feedback [45].

2.2.3. *Targeting moieties orchestrate the precise localization of PSs to disease-specific targets within pathological skin microenvironments*

Targeting moieties, such as antibodies and ligands, can be used to develop functionalized carriers or conjugates for precision delivery of PSs to disease-specific biomarkers (e.g., EGFR, CD44, IL-23R) within cutaneous pathologies [46–48]. By leveraging molecular recognition mechanisms, this strategy achieves pathogenic molecule/cell-level spatial resolution. It can bypass limitations of traditional targeting mechanisms that rely on passive diffusion or on responses to changes in microenvironment (e.g., pH/ROS level), which often suffer from targeting inaccuracies due to fluctuating pathological gradients.

Ligand-functionalized PS carriers, which represent the most extensively employed targeted delivery systems, exploit modular ligand-receptor interactions to achieve subcellular precision in PDT. These interactions include folic acid with the folate receptor, which is overexpressed in the membranes of skin tumor cells [49]; RGD with integrin $\alpha v\beta_3$, a key player in melanoma angiogenesis [50]; and hyaluronic acid (HA) with CD44, which is abundant in inflamed and cancerous skin cells [51]. For example, RGD-functionalized liposomes co-loaded with the PS chlorin e6 (Ce6) and capsazepine (TRPV1 antagonist) were engineered to amplify the tumor-specific ROS generation and block TRPV1-mediated pain signaling during PDT. The RGD motif selectively binds $\alpha v\beta_3$ integrins overexpressed on tumor vasculature, enhancing intracellular liposomal uptake. Delivered via hyaluronic acid-based dissolvable MNs, the RGD functionalized liposomes demonstrated outstanding effectiveness in PDT against melanoma in mouse skin, offering a paradigm for pain-managed oncology therapies [52]. In antibody-engineered PDT, PSs are either directly conjugated to antibodies (forming antibody-PS conjugates, APCs) or loaded into antibody-decorated nanocarriers (e.g., liposomes, polymeric nanoparticles) that recognize antigens specifically overexpressed in disease-associated cells. By functionalizing gold nanoparticles (AuNPs) with anti-Melanoma Inhibitory Activity (MIA) antibodies, the system achieved precise delivery of zinc phthalocyanine tetra-sulphonic acid ($ZnPcS_4$), a soluble and potential PS. The anti-MIA antibodies selectively bound MIA antigens overexpressed on melanoma cells, enhancing tumor-specific uptake and treatment efficacy [53].

Aptamer-targeted PDT represents a cutting-edge advancement in precision medicine, leveraging nucleic acid aptamers to enhance PS specificity and therapeutic control. As a short oligonucleotide sequence with a folded three-dimensional structure, aptamers can act as ligands modifiable to diseased cells [54]. In a recent study, the PS Ce6 was attached to a DNA probe containing the AS1411 aptamer for targeting the nucleolin expressed on tumor cells and a linear antisense oligonucleotide for down-regulation of Survivin expression and thus avoidance of tumor resistance to PDT. The resulting complex exhibited targeted delivery and activation, exhibiting enhanced PDT efficacy towards squamous cell carcinoma [55].

The integration of active targeting and stimuli-responsive drug release offers a transformative approach to enhance PDT efficacy while addressing tumor microenvironmental barriers. A prime example is the synergistic combination of RGD peptide-mediated active targeting and GSH-responsive drug activation, which enables spatiotemporal control over therapeutic delivery. In this paradigm, a RGD-modified platinum nanozyme co-loaded with a GSH-responsive PS prodrug was constructed. The GSH responsiveness could ensure the PS release from the nanoparticle at the tumor site, and the RGD peptide could enhance its targeting delivery and permeability in the cancer cells [56].

Beyond targeting human pathological markers, emerging strategies in photodynamic antimicrobial therapy exploit pathogen-specific molecular signatures to enhance therapeutic precision. An innovative MN patch was engineered with a dual-functionalized PS: pyridinium cations to amplify electrostatic adherence to negatively charged bacterial membranes (e.g., *Staphylococcus aureus*), and benzoxaborole moieties to selectively bind to peptidoglycan in Gram-positive bacterial cell walls. Upon dermal application, the MN could rapidly disintegrate at the wound site, releasing the above PS into the biofilm microenvironment. This targeted approach achieved the eradication of the multidrug-resistant bacterial biofilms in diabetic chronic wounds [57].

2.3. *Translational barriers and implications*

Despite their innovative designs, these material-based strategies discussed for overcoming PS spatiotemporal limitations face significant translational barriers. For MN-mediated delivery, key challenges encompass the variability in penetration depth due to heterogeneous skin anatomy, the risk of structural failure from mechanical stress, and constrained drug-loading capacities that may limit therapeutic dosing [58–60]. The promise of stimulus-responsive systems is weakened by the relatively broad specificity of their triggers (e.g., pH, enzymes), which can lead to premature or off-target release, thereby compromising spatiotemporal precision [61,62]. Similarly, active targeting via ligands is challenged by the dynamic and complex skin microenvironment. Factors such as suboptimal ligand-receptor binding affinity, rapid

clearance, and patient-to-patient variability in target biomarker expression collectively reduce in vivo targeting efficacy [63,64].

In addition, safety considerations represent a critical and non-negligible aspect in the clinical translation of biomaterials and constitute a primary bottleneck limiting the successful transition of most preclinical research findings into clinical practice. For instance, while topically applied nanoparticles are largely confined to the skin with limited systemic absorption, they may still penetrate into deeper dermal layers and exhibit localized accumulation, leading to prolonged tissue exposure [65–67]. In contrast, physical enhancement strategies such as MNs can disrupt the skin barrier more profoundly, thereby significantly increasing the risk of systemic entry. Once carriers or their payloads enter the systemic circulation, their subsequent biodistribution, metabolism, and elimination require comprehensive investigation. For materials that degrade slowly or not at all, such systematic assessment is particularly important, as they pose potential risks such as long-term retention in the body, accumulation in specific organs, and delayed clearance pathways.

The technical limitations of these strategies, along with their associated safety concerns, highlight critical directions for future research. Regarding safety considerations, precise monitoring of the in vivo transport pathways and degradation behaviors of nanomaterials via emerging technologies enables timely identification of potential safety risks, thereby providing critical data for risk mitigation [68,69]. Furthermore, with the ongoing advancement of AI and organoid technologies, the prospective prediction of biomaterials' in vivo exposure risks using large-scale models holds promise for circumventing research and development challenges at an early stage and substantially accelerating their clinical translation [70]. Also, future efforts should focus on combining multiple delivery strategies to enhance the precision of therapeutic transport, while incorporating real-time monitoring and dynamic adjustment capabilities throughout treatment. Illustratively, Fu et al. developed barbed MNs via advanced 3D printing for wound monitoring and drug delivery, enabling real-time intervention based on the wound state [71]. Similarly, Gu's team designed a MN patch for growth hormone that improves bioavailability through rhythmic release profiles [72]. Such advances underscore the potential of physiologically responsive, closed-loop systems. Integrating sensing, feedback, and regulation within future delivery platforms will substantially enhance the precision and adaptability of PDT, offering meaningful clinical benefits.

3. Hypoxia-mediated therapeutic resistance and material-based strategies

3.1. Hypoxia in dermal PDT

Oxygen plays a pivotal role in PDT, acting as the source of the cytotoxic ROS, particularly the singlet oxygen ($^1O_2$) generated by the Type II photochemical pathway. While both Type I and Type II reactions can occur concurrently, their relative predominance is governed by the properties of PSs, the characteristics of substrates, and the availability of oxygen. However, most of the reported PSs are Type II dependent, and unfortunately, hypoxia is an intrinsic hallmark of many dermatological diseases, such as malignant solid tumors and chronic wounds. The oxygen tension (pO_2) in most solid tumors typically ranges below 5 mmHg, starkly contrasting with the physiological norm of 10–80 mmHg in healthy tissues [73]. In contrast to normal skin tissue, where the pO_2 is maintained in the range of 35–50 mmHg, chronic wounds also exhibit markedly reduced oxygen levels (5–20 mmHg), with values plummeting further to 0–10 mmHg in the hypoxic wound core [74].

The oxygen present in the skin arises from two primary pathways, namely the centrifugal oxygen diffusion from subcutaneous vasculature, where oxygen carried by dermal capillaries passively diffuses outward to nourish epidermal layers, and the atmospheric oxygen permeation, with environmental oxygen traversing the stratum corneum to supplement superficial epidermal oxygenation (Fig. 3). This dual-source mechanism establishes distinct physiological oxygen gradients across skin layers: a centrifugal gradient decreasing from the oxygen-rich hypodermis to the metabolically active dermis, and a superficial gradient decreasing from the stratum corneum to the stratum basale due to the transepidermal oxygen diffusion [75]. As shown in Fig. 3, the well-vascularized dermis maintains a physiological pO_2 of ~10 %, while the epidermis exhibits a descending gradient from moderately hypoxic (pO_2 ~5 %) in superficial layers to moderately or severely hypoxic microenvironments (pO_2 <1 %) within pilosebaceous units (e.g., hair follicles, sebaceous glands) [76]. In accordance, two approaches can be used to increase the oxygen supply to the local skin: inhalation of gaseous oxygen via the respiratory tract and topical delivery of oxygen. While respiratory oxygenation ensures whole-body supply, its delayed cutaneous effects limit its utility in acute dermatological interventions accompanied by vascular damage. In contrast, topical oxygen therapies bypass systemic delays by directly elevating cutaneous pO_2 through stratum corneum permeation [77]. Especially, it has been demonstrated that the superficial skin layers (0.25–0.40 mm depth) are primarily oxygenated through atmospheric diffusion via transepidermal oxygen permeation, whereas vascular-derived oxygen from blood capillaries plays a negligible role in this region [78].

Intrinsically, the skin has a certain ability to regulate oxygen homeostasis through a coordinated network of molecular, vascular, and metabolic pathways that dynamically adapt to environmental and physiological challenges. Central to this regulation is the hypoxia-inducible factor (HIF-1α) pathway, which is stabilized under conditions of hypoxia to drive angiogenesis, vascular blood flow, glycolytic metabolism, and erythropoiesis, enhancing oxygen delivery and utilization in hypoxic disorders such as chronic wounds [79]. HIF-1α stability and activity are tightly regulated by oxygen-dependent hydroxylases. Under normoxia, prolyl hydroxylases (PHD1-3) hydroxylate HIF-1α at specific proline residues (Pro402/Pro564), marking it for von Hippel–Lindau tumor suppressor protein (VHL)-mediated proteasomal degradation. Asparaginyl hydroxylase FIH-1 leads to the hydroxylation of asparagine 803 in the HIF-1α, further suppressing its transcriptional activity by blocking co-activator (p300/CBP) binding. As oxygen levels decline, PHD/FIH-1 activity diminishes due to substrate (O_2) limitation and mitochondrial ROS-mediated oxidation of Fe(II) in their catalytic centers, stabilizing HIF-1α. PHD2 preferentially targets HIF-1α, while PHD1/3 favor HIF-2α. Stabilized HIF-1α translocates to the nucleus, dimerizes with HIF-1β, recruits p300/cyclic-AMP response element binding protein (CBP), and activates hypoxia-response genes regulating angiogenesis, metabolism, and survival. This oxygen-sensing cascade enables adaptive responses to hypoxia through transcriptional reprogramming [80,81].

3.2. Material-based strategies

Strategies to address hypoxia in PDT can be primarily categorized into three approaches, including structural optimization of PSs, combination with hypoxia-activated prodrugs, and direct oxygen supply or generation. The first two represent “adaptive” strategies, either modifying the PS to maintain activity under low oxygen or designing prodrugs in which the PS is chemically linked or physically co-delivered with a chemo-/immunotherapeutic agent [82]. The former aims to preserve the intrinsic photodynamic action under hypoxia, while the latter leverages the PDT-augmented hypoxic microenvironment to trigger a combined therapeutic response [83–86]. However, these approaches often face significant synthetic complexity, potential systemic toxicity, and mechanisms that extend beyond the core photodynamic action. In contrast, material-based “active oxygen-replenishing” strategies offer a more direct and controllable solution by actively alleviating hypoxia in situ, thereby enhancing PDT in a more targeted and efficient manner [87]. Accordingly, the following sections provide a systematic evaluation of these material-based approaches, including natural

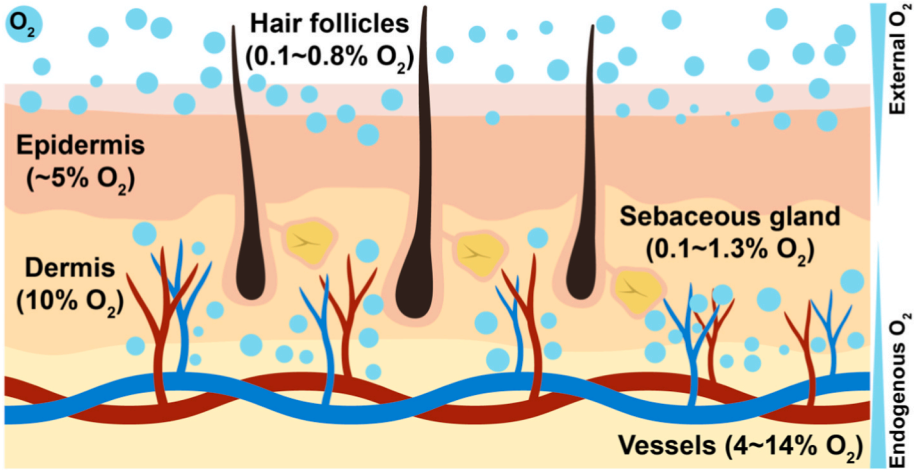

Fig. 3. The oxygen level and gradient characteristics across different skin tissues.

enzymes, nanozymes, oxygen-loaded carriers, oxygenic precursors, and photosynthetic materials (Table 2), with emphasis placed on their design principles, translational potential, and remaining challenges.

3.2.1. Topical application of external catalase enables transdermal O_2 delivery based on catalase-based biochemical reactions

Topical application of catalase-based formulations represents an innovative strategy to overcome hypoxia in PDT by enabling enzymatic oxygen generation directly within the H_2O_2 over-expressed microenvironment. Previous studies have shown that a high amount of native catalase is present in the skin, which can effectively catalyze the topical H_2O_2 to O_2. However, it requires a high concentration of peroxide substrate (0.5–1 mM H_2O_2) to generate a substantial amount of O_2, which may cause severe skin burn and blistering [88,89]. In addition, the expression of catalase would be significantly decreased in the case of skin disorders like vitiligo and UV radiation [90,91]. Fortunately, topical application of catalase effectively enhances cutaneous oxygenation, achieving dozens of times reduction in H_2O_2 concentration.

To address the hypoxic limitation of PDT in bacterial infections (e.g., *Staphylococcus aureus*) in the skin, a PS (Ce6)-catalase conjugate was developed and dermally delivered via incorporation into the fluorinated polyethylenimines (F-PEI) to form the transdermal nanoparticles for enhanced PS delivery. The system showed a unique advantage in the penetration depth through the skin by comparison with non-fluorinated counterparts. The in vivo abscess animal model demonstrated that topical application of Ce6-CAT@F-PEI, followed by light irradiation, could trigger the decomposition of H_2O_2 for O_2 self-supply and achieve highly effective PDT towards *Staphylococcus aureus* [92].

To enhance antitumor efficacy by PDT, Huang et al. engineered a self-oxygenating MN patch via simultaneous incorporation of the catalase and the PS, such as 5-ALA and 2-(1-hexyloxyethyl)-2-divinylpyropheophorbic-a. For further achieving the ion-interference effect (e.g., Cu^{2+}/Ca^{2+} respectively for GSH depletion and oxidative stress-mediated apoptosis) and the sustained release effect, metal-based nanoparticles such as the Cu^{2+} doped calcium phosphate nanoparticles and zeolitic imidazolate frameworks (Fig. 4a and b) could be used as their carriers, providing sufficient loading and encapsulation. In response to the increased oxygen, ALA-synthetase (ALAS) would be up-regulated via a heme negative feedback mechanism (Fig. 4c). To evaluate hypoxia alleviation and PS efficacy, intracellular oxygen generation was assessed using the RDPP probe, revealing an almost 30 % reduction in fluorescence (FL) signal for CAT-loaded nanoparticles, confirming CAT-mediated O_2 production via H_2O_2 decomposition (Fig. 4d–f). For 5-ALA/CAT-loaded nanoparticles, the generation of PpIX was significantly improved after 24 h post-incubation, achieving 4 times as high as the PpIX FL intensity when 5-ALA alone was used (Fig. 4g–i). Real-time PpIX metabolic profiling showed 5-ALA/CAT-loaded nanoparticles (CCPCA) delayed peak FL intensity to 24 h (vs. 6 h for 5-ALA; 10 h for no CAT-loaded nanoparticles), extending the metabolic time window for repeatable PDT (Fig. 4j). Catalase-mediated elevation of endogenous O_2 levels inhibited the expression of HIF-1α under both normoxia (21 % O_2) and hypoxia (1 % O_2) conditions with time- and concentration-dependent profiles (Fig. 4k–n). The down-regulation of HIF-1α would amplify PpIX accumulation via reduction of ferrochelatase (FECH) expression and protoporphyrin IX (PpIX) efflux, but upregulation of ALAS. This dual CAT/PS co-delivery system synergistically resolves hypoxia, enhances PpIX accumulation, and prolongs therapeutic activity, enabling precision PDT with sustained efficacy [30,93].

However, the topical application of enzymatic formulations faces significant challenges due to their inherent instability and rapid activity loss during storage and application. While nanocarrier-based immobilization strategies offer partial mitigation, these methods often fail to fully address sustained enzymatic activity during practical use, particularly in chronic dermatological treatments requiring prolonged

Table 2
Comparative analysis of hypoxia-alleviating strategies in cutaneous PDT.

Approaches	Example	Mechanism	Advantage	Limitation
Natural enzymes	catalase-PS conjugate or co-loaded system	catalyze $H_2O_2 \rightarrow H_2O + O_2$	high catalytic specificity; biocompatibility	enzyme denaturation; Immunogenicity; limited tissue penetration
Nanozymes	MnO_2 and prussian blue nanoparticles		stable, tunable activity, low cost, and scalability	potential toxicity, multi-enzymatic properties
Oxygen-loaded carriers	hemoglobin, perfluorocarbon, and MOF	encapsulate/load and release molecular O_2	high O_2 capacity; sustained release; biocompatibility	potential toxicity; high cost
Oxygenic precursors	H_2O_2, CaO_2, MgO_2, and $2Na_2CO_3{\cdot}3H_2O_2$	hydrolyzed or decomposed to generate O_2	high O_2 yield; water-triggered release	rapid O_2 depletion; pH elevation
Photosynthetic materials	cyanobacteria	photosynthetic O_2 generation under light	continuous O_2 supply	immune clearance; light penetration limitations

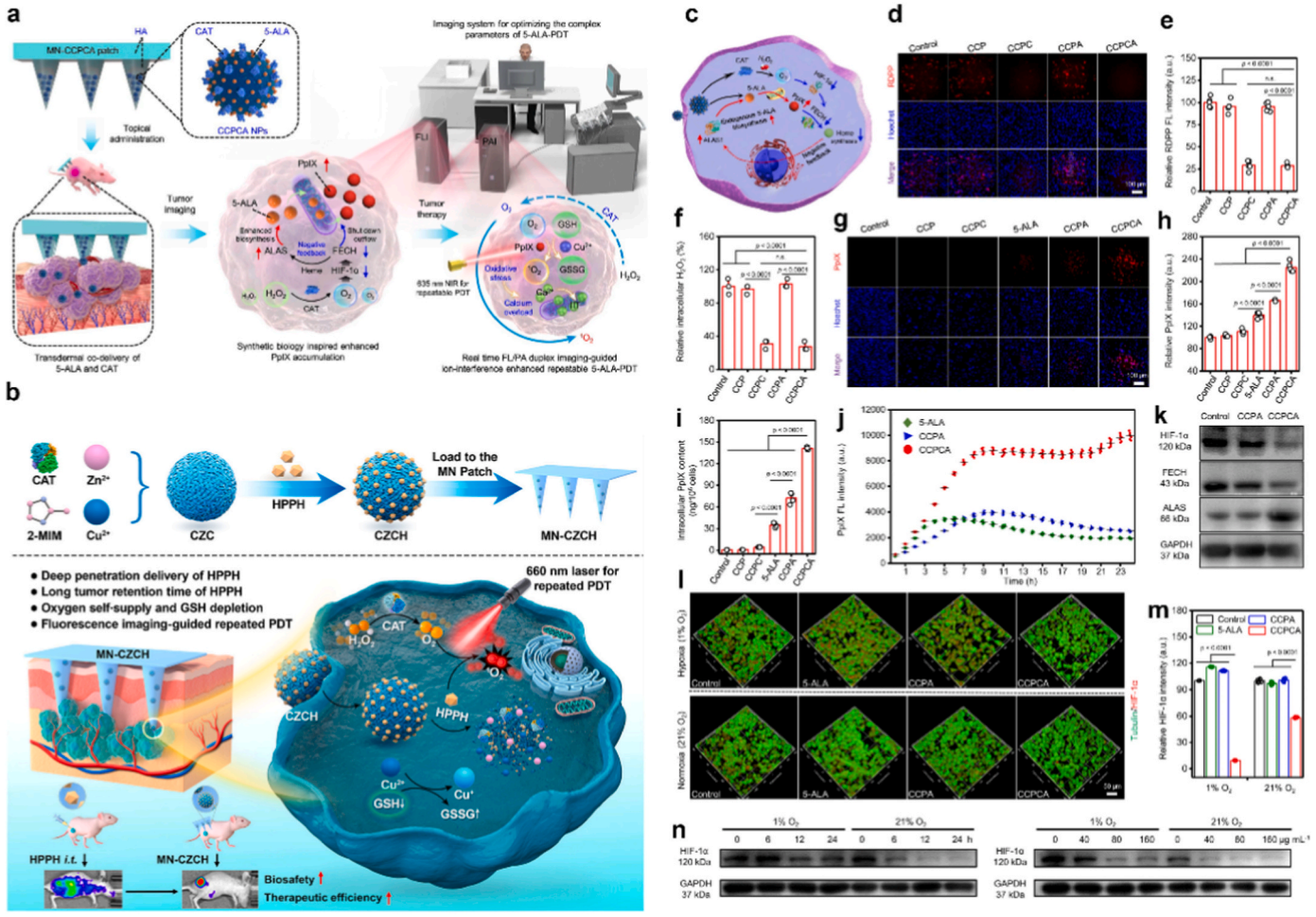

Fig. 4. MNs containing CAT/PS-loaded nanoparticles for improvement of PDT, including (a) the MN containing 5-ALA/CAT co-loaded copper-doped calcium phosphate nanoparticles (CCPCA), (b)the MN containing 2-(1-hexyloxyethyl)-2-divinylpyropheophorbic-a (HPPH)-loaded zinc imidazolate framework (ZIF), (c) increased intracellular O_2 induced PpIX accumulation through a heme negative feedback mechanism, (d, e) FL images and quantitative analysis of RDPP after treatment by different nanoparticles at equivalent concentrations (80 μg mL^{-1}) for 24 h, scale bar = 100 μm, (f) H_2O_2 levels in A375 cells, (g, h) FL images and quantitative analysis of PpIX in A375 cells after treatment by equivalent amounts of free 5-ALA (5.4 μg mL^{-1}) or 80 μg mL^{-1} nanoparticles, scale bar = 100 μm, (i) intracellular PpIX content in the lysate, (j) Real-time FL quantitative analysis of PpIX metabolism, (k) real-time FL quantitative analysis of PpIX metabolism, (l, m) immunofluorescence images and quantitative analysis of anti-α-tubulin (green) and anti-HIF-1α (red) in A375 cells, (n) western immunoblots analysis of HIF-1α expression at different time and concentrations. Copied with permission [30,93]. Copyright 2022, Springer. Copyright 2022, ACS.

therapeutic windows [94,95]. PEGylation of catalase has recently been proposed to increase its stability. The PEGylated CAT was demonstrated to increase half-life by > 5-fold, although PEGylation reduced specific activity (more pronounced with higher *MW* PEGs) [96].

3.2.2. Nanozymes can substitute natural catalase in PDT and produce catalase-like oxygenous effect

The emergence of nanozymes with enzyme-mimicking activities has revolutionized healthcare and biomedicine, offering distinct advantages over natural enzymes, such as superior stability, tunable catalytic activity, and cost-effective scalability. Among these, the catalase nanozyme with H_2O_2-decomposing capability has garnered significant attention, enhancing oxygen supply in hypoxic microenvironments, a critical barrier in therapies like PDT [97,98].

The initial report of catalase-mimetic nanozymes was first published in 2009, when core-shell Au/Pt bimetallic nanoparticles were found to have dual superoxide dismutase- and catalase-like activities, offering therapeutic potential for oxidative stress-related pathologies [99]. Subsequent advancements have expanded this field to encompass diverse nanomaterials, including metal-based, metal oxide-based, MOF-based, and carbon-based nanomaterials [100]. Among the diverse nanozyme platforms, metal-based nanoparticles, particularly those incorporating platinum (Pt), manganese (Mn), and gold (Au), are predominantly employed due to their superior catalytic efficiency, biocompatibility, and multi-enzyme activity, making them ideal candidates for hypoxia-alleviated PDT.

Specifically, Mn-based nanozymes, leveraging their robust catalase-mimetic activity, have become the foremost candidates for enhancing PDT in dermatology, particularly in treating hypoxic skin tumors and chronic wounds through the in situ oxygen generation [101]. They can be integrated into PDT systems through three principal configurations: Mn-doped composites, manganese dioxide (MnO_2) nanostructures, and Mn-porphyrin coordination complexes (e.g., Mn-based metal-organic frameworks, MOFs). Among them, MnO_2 nanoparticles stand out as the most widely employed agents for hypoxia alleviation in PDT, owing to their excellent CAT-like activity. For example, MnO_2 nanoparticles and the PS Ce6 were co-loaded into a polymeric nanocarrier coated with polyethylene glycol (PEG). Under hypoxic nitrogen atmospheres, the addition of H_2O_2 markedly enhanced the light-triggered singlet oxygen ($^1O_2$) generation by Ce6@MnO_2-PEG nanoparticles, restoring $^1O_2$ yields to levels comparable to those achieved by free Ce6 or Ce6@MnO_2-PEG nanoparticles under normoxic (air) conditions. Furthermore, the Mn^{2+} ions released during nanoparticle degradation function as an adjuvant-like stimulator to activate the host immune system. This

immunomodulatory effect synergizes with light-triggered PDT, enabling both clearance of *S. aureus*-induced skin abscesses and long-term immunological memory against reinfection [102]. Simultaneously, the substantial released Mn^{2+} ions can be utilized to enhance T1-magnetic resonance (MR) imaging contrast for all-in-one theranostic tools due to the tumor-specific imaging capacity [103]. In addition, MnO_2 nanoparticles can be further hybridized with other metals (e.g., Cu, Pt, Au) to enable multi-enzyme catalytic cascades (e.g., catalase-, peroxidase-, oxidase-like activities) for amplified oxidative damage, while simultaneously achieving photothermal (PTT)-PDT synergy under near-infrared (NIR) irradiation. For instance, Li et al. engineered a nanocomposite (Cu-TCPP@MnO_2) which enabled the triple-modal synergistic therapy including PDT, PTT, and chemodynamic therapy (Fig. 5a). After topical application, the two-dimensional Cu-TCPP nanosheets could not only act as the PS to produce ROS (Fig. 5b), but also as the photothermal agent to convert light energy into heat under dual-laser radiation. The produced PTT effect would also enhance the ROS generation during PDT, promote the release of metal ions (Mn^{2+} and Cu^{2+}) serving as the reactant in Fenton-like reactions to convert H_2O_2 into hydroxyl radicals (•OH) and consuming the overexpressed GSH to reduce the ROS scavenging effect (Fig. 5c–i), and accelerate the catalysis of H_2O_2 into O_2 by MnO_2 (Fig. 5j). These synergistic effects have shown remarkable bactericidal properties for infected wound healing [104].

Recently, Prussian blue (PB) nanoparticles, a type of iron-based metal-organic framework, have emerged as multi-enzyme mimics with excellent catalase, superoxide dismutase, and peroxidase-like activities for ROS scavenging due to the redox-active Fe^{2+}/Fe^{3+} centers [105]. Typically, PB has a chemical formula of $Fe_4[Fe(CN)_6]_3$ [IUPAC name: Iron (II, III) hexacyanoferrate (II, III)]. In the presence of H_2O_2, the PB nanoparticles exhibit a shift in the catalytic behavior from POD to CAT as the pH transitions from acidic to neutral conditions [106]. In addition, unlike other nanozymes exhibiting depletable catalytic activity, the enzyme-like activities of PB nanoparticles can be well maintained and even slightly enhanced over time, which may be due to the pre-oxidation effect of H_2O_2 and the subsequent increase in the valence state of surface Fe [107]. Tong et al. developed Ce6-loaded PB nanoparticles that synergistically integrate catalase-mimetic activity with PDT. This dual-functional platform ensured the effective eradication of *MRSA* due to the hypoxia alleviation (4 times enhancement in oxygen production). After topical use, the *MRSA*-infected mice revealed accelerated wound healing through VEGF-mediated tissue regeneration, while maintaining favorable biosafety profiles [108].

3.2.3. Oxygen-loaded carriers enable localized cutaneous oxygen supplementation for improvement of PDT

Oxygen-loaded carriers represent a transformative class of biomaterials engineered to address hypoxia-related pathologies through precision-controlled gas transport. These systems, encompassing hemoglobin (Hb)-based vesicles, perfluorocarbon (PFC)-based carriers, and synthetic oxygen-loaded materials such as MOF, actively modulate tissue oxygenation due to the high oxygen affinity and stimuli-responsive release properties [109,110]. For example, leveraging the near-infrared (NIR)-responsive photothermal conversion, the black phosphorus quantum dot modified MNs encapsulating Hb achieve the temperature-modulated oxygen release, since the generated heat would decrease the oxygen binding capacity of Hb. Each hemoglobin molecule exhibits a tetraoxygen-binding capacity, with oxygen-loading efficiency demonstrating a positive correlation to the encapsulation efficiency of the Hb. Critically, the dissolved oxygen pressure demonstrated stable even after the complete release of oxygen, confirming the maintenance of release equilibrium and no detectable reabsorption (Fig. 6a) [111].

As chemically inert organofluorine compounds, PFCs act as artificial red blood cells with exceptional oxygen solubility [114]. Perfluorooctyl bromide and perfluorodecalin are the two most commonly used PFCs as oxygen carriers, which can respectively dissolve 527 and 403 mL O_2/L PFC compared to 9–10 mL O_2/L water in water and 200 mL O_2/L blood in blood at 1 atm [115]. When formulated into a nanoemulsion, perfluorooctylbromide could achieve targeted supply of oxygen to the hair follicle through the skin for promoting hair growth under anoxic conditions [116]. Simultaneously, the chitosan-based dressings conjugated with PFC were found to deliver and sustain oxygen for the enhancement of wound healing after topical use [117–119]. In addition, it was suggested that the PFC-engineered nanodroplets incorporating the drug rifampicin and the PS indocyanine green could address antibiotic resistance in acne vulgaris by synergizing photodynamic, chemotherapeutic, and probiotic actions. Leveraging PFC's oxygen-rich microenvironment, the system achieved increased $^1O_2$ generation for amplified PDT efficacy against *Propionibacterium acnes* under NIR irradiation (808 nm) [120].

3.2.4. Oxygenic precursors ameliorate hypoxia through self-decomposing reaction or hydrolysis

Oxygenic precursors represent a class of chemically active materials capable of autonomous oxygen generation through self-decomposition or hydrolysis reactions, offering on-demand hypoxia alleviation in biomedical applications. Beyond conventional liquid peroxides such as hydrogen peroxide (H_2O_2), solid-state metal peroxides, including calcium peroxide (CaO_2), magnesium peroxide (MgO_2), and sodium percarbonate (SPC, $2Na_2CO_3{\cdot}3H_2O_2$), can also serve as oxygen reservoirs [110].

By integrating sodium percarbonate with poly(vinyl pyrrolidone) MNs loaded with Ce6, the system achieved gas-driven PS delivery in the skin tissues and hypoxia alleviation. As an oxygen propellant, SPC could react with the surrounding fluid to generate oxygen bubbles upon hydration, creating convective fluid flows that increased Ce6 penetration from 918 μm to 1130 μm. Simultaneously, oxygen release boosted ROS production and enhanced the PDT effect towards the hypoxic breast cancer cells under irradiation. In vivo studies on an intradermal breast cancer mouse model demonstrated the tumor growth suppression in murine models after 20-day treatment, attributed to synergistic effects of accelerated PS permeation and sustained oxygen supply (Fig. 6b) [112].

3.2.5. Photosynthesis can be utilized as an oxygen-evolution method for oxygen replenishment

As the largest oxygen-producing system existing in nature, photosynthesis can produce oxygen based on photosynthetic microorganisms, chloroplasts, or thylakoids, among which photosynthetic microorganisms are most used. A photosynthetic oxygen generation system comprises three core components: (1) photosynthetic microorganisms as the oxygenic reaction subject, (2) biocompatible carriers for localized and deep delivery, and (3) tunable light sources (400–750 nm) to driven situ oxygen replenishment [121]. By comparison with other methods, this approach can avoid the toxicity of toxic ionic products such as Mn^{2+} and keep stable activity under the harsh and complex pathological environments [122,123].

Cyanobacteria, the earliest photosynthetic bacteria on Earth, can utilize water as an electron donor to reduce CO_2 into organic carbon compounds while releasing oxygen under sunlight. As natural oxygen carriers, their unique oxygen-evolving capability has been applied to avoid the hypoxic issue in the PDT [122,124]. For instance, an innovative dual-layered hydrogel system was developed by integrating cyanobacteria-driven oxygen production with PDT to address the challenges of hypoxia for PDT of bacterially infected diabetic wounds. The outer hydrogel layer harnesses photosynthetic cyanobacteria to continuously generate oxygen under natural light, effectively alleviating tissue hypoxia and creating an oxygen-enriched microenvironment. This sustained oxygenation synergizes with the inner layer's photodynamic MOF (i.e., PCN-224), amplifying ROS generation to eradicate resilient bacterial biofilms. Beyond enhancing antimicrobial efficacy, the cyanobacteria-derived oxygen promotes critical regenerative processes: accelerating cell migration, suppressing chronic inflammation, and

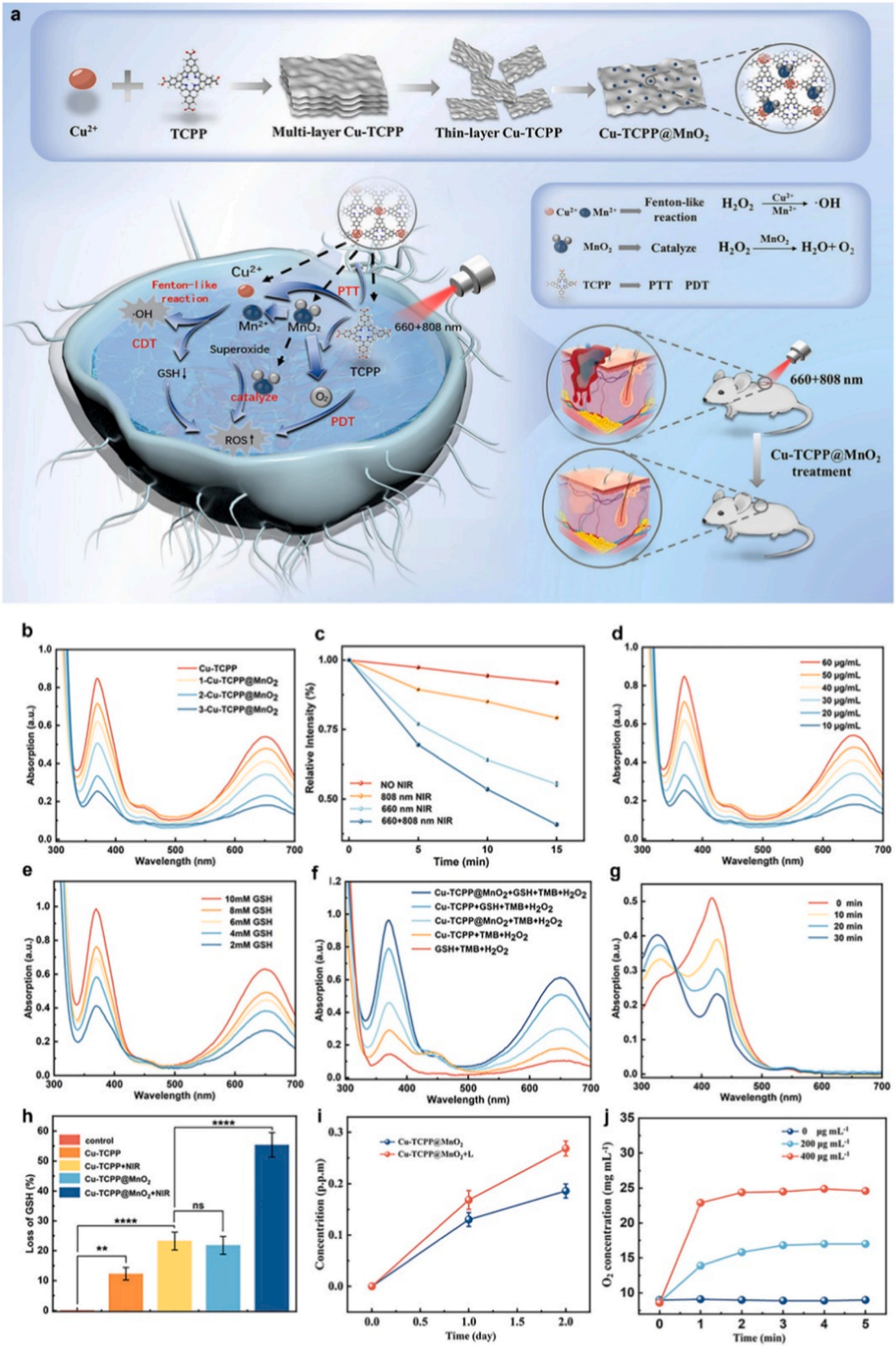

Fig. 5. Cu-TCPP@MnO_2 nanocomposites for synergistic treatment, including (a) scheme of synthesis process and mechanism of the synergistic action, (b) ROS yields of Cu-TCPP and x-Cu-TCPP@MnO_2 with different copper content under dual laser irradiation, (c) Relative intensity of ROS generated by Cu-TCPP@MnO_2 under different conditions, (d) •OH yield of Cu-TCPP@MnO2 at different concentrations, (e) •OH yield at different GSH concentrations, (f) •OH production at different conditions, (g) •OH consumption with the reaction time, (h) depletion of GSH at different conditions; (i) the release of Cu^{2+} with and without illumination; (j) the concentration of oxygen in presence of Cu-TCPP@MnO_2 at different concentrations. Copied with permission [104]. Copyright 2025, Elsevier.

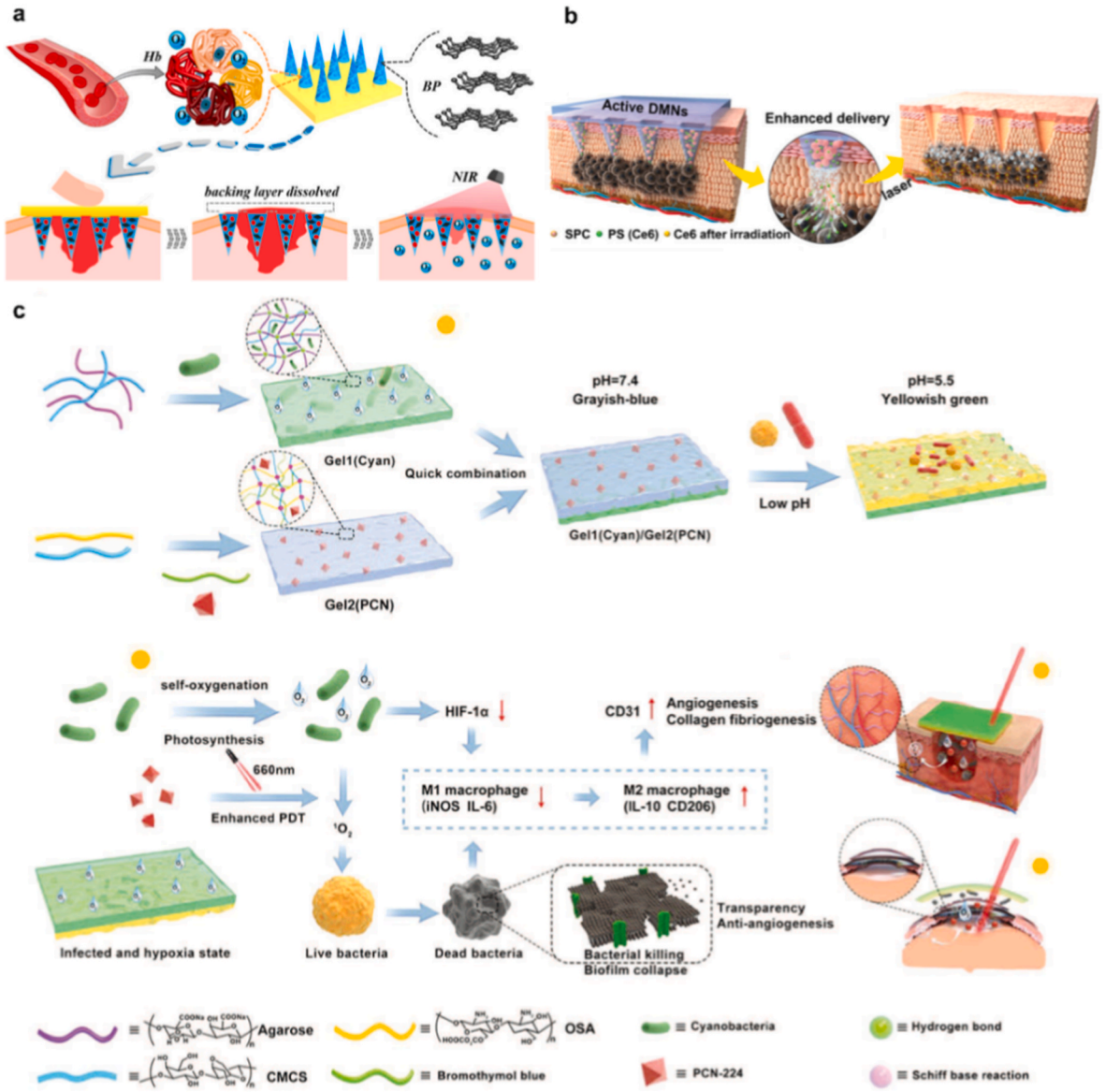

Fig. 6. Non-metabolic strategies for enhancing oxygenation in cutaneous PDT, including (a) oxygen carriers (e.g., Hb), (b) precursors (e.g., SPC), and (c) photosynthesis (e.g., cyanobacteria). Copied with permission [111–113]. Copyright 2020, ACS. Copyright 2022, Wiley. Copyright 2022, Wiley.

stimulating angiogenesis. By bridging hypoxia mitigation, infection control, and tissue repair, this biohybrid platform demonstrates a self-sustaining therapeutic strategy that leverages cyanobacteria's innate photosynthetic capability to transform wound management (Fig. 6c) [113].

3.3. Translational barriers and implications

While the strategies discussed above offer promising avenues to alleviate hypoxia in PDT, each faces distinct developmental and translational challenges [125]. Natural enzymes are limited by poor delivery efficiency, non-specific accumulation, and a lack of spatiotemporal control [126]. Nanozymes, though more stable, generally exhibit inferior catalytic efficiency compared to their natural counterparts, and the mechanisms governing their activity regulation are not fully elucidated. The molecular basis for synergy in multi-enzyme systems, especially where substrate competition exists, remains poorly defined, necessitating deeper study into electron transfer pathways and microenvironmental modulation. Off-target effects due to insufficient specificity further complicate their application. Critically, the biosafety of metal-based nanozymes constitutes a major concern. The potential for metal ion leakage, tissue accumulation, and collateral damage resulting from Fenton-like reactions necessitates thorough evaluation. It is crucial to precisely quantify the in vivo dosage, biodistribution, and clearance kinetics of these metallic components, particularly those with potential toxicity, to ensure safety [127,128].

Oxygen carrier strategies, which primarily function as passive reservoirs, encounter significant challenges in stability and control. These include the physical and chemical stability of the carrier materials themselves, the stability of their oxygen-loading capacity during storage and circulation, and critically, the spatiotemporal stability of oxygen release rates. Often, the release profile fails to align with the rapid and fluctuating oxygen consumption rates within tumors, leading to inefficient reoxygenation [129]. Furthermore, the adverse effects associated with these carriers are not fully characterized, their clinical indications remain inadequately defined, and a more comprehensive understanding of their in vivo metabolic fate and tissue oxygenation efficacy is required. Oxygenic precursors contend with challenges such as excessively rapid reaction kinetics and byproducts that can alter the microenvironment. Photosynthetic materials, such as cyanobacteria, as living

systems, encounter significant obstacles related to immunogenicity and limited light penetration depth [130].

In the future, with the deep integration of materials science and life sciences, the development of safer and more stable nanozymes and self-oxygen-supplying systems is anticipated to effectively mitigate the hypoxic microenvironment in PDT, thereby further enhancing its therapeutic efficacy. For instance, an engineered cyanobacterium designed and constructed using synthetic biology approaches, when modified with MnO_2, exhibits stable oxygen generating capacity and enables synergistic integration of PDT and immunotherapy [131]. Ultimately, achieving a safe, efficient, and precisely controllable oxygen supply will be pivotal for advancing the clinical translation of next-generation PDT.

4. Light-related issues and material-based strategies

4.1. Limited light penetration in the skin and spectral mismatch with other phototherapy

Therapeutic light irradiation serves as the cornerstone of PDT, not only activating PSs through precise wavelength-tuned photon delivery but also functioning as a versatile platform for multi-modal phototherapeutic integration [8]. Usually, by employing distinct yet coordinated wavelengths, PDT and PTT can be synergistically integrated to enable complementary therapeutic action while overcoming the inherent limitations of monotherapy. The thermogenic effect elicited by PTT potentiates the PDT efficacy through dual mechanisms: (1) hemodynamic modulation via localized hyperthermia enhances microvascular perfusion and vascular permeability, facilitating oxygen and PS delivery; (2) proteostatic disruption through ROS-mediated oxidation of heat-shock proteins (HSPs, e.g., HSP70/90), the molecular chaperones critical for DNA repair and anti-apoptotic signaling, thereby sensitizing cancer cells to PDT-induced oxidative stress [132].

A fundamental challenge in light-based dermatological therapies lies in overcoming the skin's stratified optical barriers, which impose wavelength-dependent limitations on effective light penetration [133]. The depth of light penetration into cutaneous tissue exhibits a biphasic relationship with wavelength, and it progressively increases from the ultraviolet (200–400 nm) through visible (400–750 nm) spectra before declining in longer infrared wavelengths (750–1000 nm) due to the water absorption. During transdermal light propagation, the optical energy density undergoes nonlinear attenuation with increasing tissue depth, stemming from the dual mechanisms of photon absorption and scattering within cutaneous layers. For example, the ultraviolet radiation at 300 nm demonstrates limited cutaneous penetration, with 37 % of incident photons attaining depths of 15 μm (epidermal stratum corneum), while 340 nm wavelengths achieve deeper permeation (54 μm) into the viable epidermis. In the visible to near-infrared spectrum, 450 nm and 650 nm light demonstrate 1 % residual fluence rate at depths of 1.6 mm (superficial dermal plexus) and 5.2 mm (subcutaneous adipose interface), respectively [134]. Therefore, optimal therapeutic outcomes in cutaneous PDT necessitate precise optimization of optical parameters, requiring sufficient fluence at critical depths while maintaining wavelength-specific biocompatibility. In addition, the implementation of synergistic PTT-PDT combination therapy also requires precise spectral congruence to simultaneously activate PSs and photothermal agents, thereby enabling spatiotemporal coordination of ROS generation and hyperthermia effects within an identical treatment modality.

4.2. Material-based strategies

Based on the above discussion, this section outlines material-based strategies to address the three key challenges related to light of cutaneous PDT: shallow light penetration, inaccurate spatial delivery, and limited treatment flexibility. Specifically, skin optical clearing agents enhance photon travel through tissue; MN-based systems provide precise intradermal illumination; and miniaturized LEDs offer portable, on-demand activation. These innovations improve targeting precision, treatment control, and usability, advancing PDT for more efficient and accessible clinical use.

4.2.1. The skin optical clearing agent enhances light penetration and absorption in target tissue layers to optimize the utilization of light in PDT

The skin optical clearing (SOC) technique represents a biomedical method that enhances the transparency of the skin tissue by temporarily reducing optical scattering, enabling improved light penetration and absorption in the local skin tissue for diagnostic or therapeutic purposes. This is usually achieved through the application of optical clearing agents (OCAs) such as glycerol, propylene glycol, or hyperosmotic solutions, which penetrate the skin, alter its refractive index, and dehydrate cellular components to minimize light scattering during PDT [135,136]. However, the stratum corneum (SC) acts as a critical barrier, impeding the penetration of OCAs into deeper skin layers and thereby compromising optical clearing efficacy. To address this limitation, strategies such as mechanical methods (e.g., tape stripping), chemical permeation enhancers, and physical devices (e.g., microneedling) have been developed to enhance OCA delivery and optimize tissue transparency [137,138].

Among several common chemical permeation enhancers (Azone, oleic acid, and propylene glycol), oleic acid exhibited the strongest enhancement effect on the transdermal penetration of the OCA glycerol in a Carbomer 940 gel matrix, with the effect escalating proportionally with concentration until reaching a maximum efficacy at 4.0 wt% (Fig. 7a–c). Treated by the SOC gel, the porcine skin gradually became transparent with the prolongation of the treatment time, indicating its optical clearing effect in the visible light window (Fig. 7d). The in vivo study confirmed the reversible nature of this optical clearing effect: the 533 nm light transmittance of mouse skin increased from approximately 35 %–60 % upon SOC gel application and returned to baseline levels (37 %) following a recovery period, demonstrating the transient and controllable modulation of tissue optical properties (Fig. 7e–g). Its biosafety was also confirmed by both H&E and Masson's trichrome staining results (Fig. 7h and i). In tumor eradication experiments, the experimental group demonstrated a several-fold increase in localized ROS generation efficiency compared to controls, driven by enhanced optical clearing efficacy that improved visible light penetration [139].

The MN approach can not only improve optical clearing efficacy for enhanced tissue transparency but also synergize with PDT by optimizing PS activation through precise light-tissue interactions. The minimally invasive nature of MN ensures targeted OCA deposition, reduces treatment time, and amplifies PDT outcomes while minimizing collateral damage to surrounding healthy tissues. For example, the dissolvable MN patches prepared from hyaluronic acid (HA) can be used as the OCA for minimally invasive optical clearing. The HA-MN platform (16 × 16, 1200 μm length) significantly enhanced light penetration in turbid porcine skin due to the refractive index matching, elevating 655 nm transmittance from 0.02 % to 12.13 % in vitro. This optical clearing effect facilitated high-resolution visualization of subcutaneous structures, including a 6-fold improvement in confocal imaging clarity of tattoo dyes and direct naked-eye observation of blood vessel networks in vivo. Crucially, in a simulated subcutaneous tumor model, the skin pretreatment by the HA-MN amplified the PDT efficacy towards tumor cells with ablation efficiency increased from 60.1 % to 86.9 %, demonstrating its capacity to optimize PS activation through enhanced photon utilization [140].

4.2.2. MN-based light-guiding channels direct therapeutic light delivery to the target site within the skin

Light-guiding channels represent an innovative approach for enhancing precision in phototherapy by enabling controlled delivery of therapeutic light to specific dermal regions. These specialized optical pathways, often engineered using advanced materials or

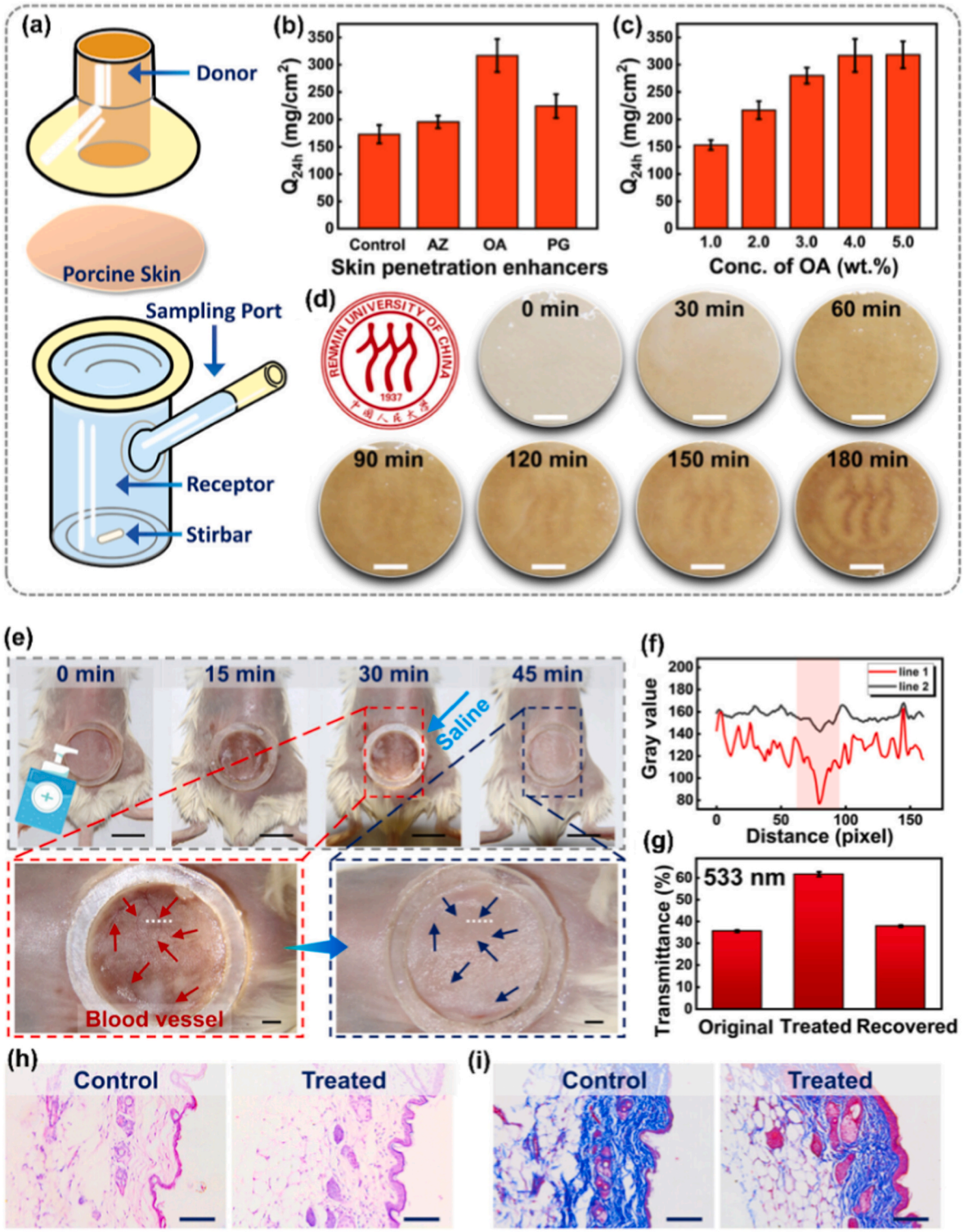

Fig. 7. Skin optical clearing technology for deepened PDT, including (a) scheme of the diffusion cell used to evaluate transdermal penetration of glycerol, (b) effect of different skin enhancers on the cumulative penetration amount of glycerol in 24 h (Q24h), (c) the permeation enhancement effects of oleic acid (OA) at different concentrations, (d) photographs of the porcine skin treated by SOC gel for different times (scale bar: 1.0 cm), (e) photographs of living mice skin treated by SOC gel for different time (scale bar: 1.0 cm in the original photograph, 2.0 mm in the enlarged pictures), (f) Gray value analysis of the white dashed line in the enlarged photograph e (line 1: left, line 2: right), (g) transmittance of the untreated and treated mice skin by the SOC gel treatment for 30 min and the recovered skin, (h) histological hematoxylin-eosin (H&E) staining of the SOC gel-treated mice skin tissue (scale bar: 100 μm), (i) Masson's trichrome staining of untreated and SOC gel-treated mice skin tissues (scale bar: 100 μm). Copied with permission [139]. Copyright 2024, ACS.

microstructured devices, optimize light transmission through skin layers while minimizing scattering and absorption in non-target tissues [141].

Transparent MN arrays can be engineered to function as dual-purpose, self-contained light-guiding channels, where the MN body itself serves as an optical conduit for direct therapeutic light delivery. By fabricating MNs from optically transparent and biocompatible materials, the needle structure inherently transmits light from its base to the tip with minimal loss, effectively merging the mechanical penetration and light-delivery functions into a single unified system. This design obviates the necessity for distinct light guiding components, enabling the physical channel of the MN, established upon insertion into the skin, to concurrently direct light to specific subdermal targets [142].

To mitigate optical interference caused by the payloads in the MN, particularly the light-scattering effects of nanoformulated therapeutics, a strategic hierarchical configuration can be implemented, where the nanotherapeutic PSs are selectively deposited at the MN tip, while the remaining shaft is fabricated from a pristine, optically transparent matrix material. This compartmentalized design preserves the MN's light-guiding performance by isolating light-scattering drug components to the tip region, ensuring unimpeded light transmission through the transparent body. For example, Zhao et al. developed a dual-function MN array consisting of a dissolvable needle tip (height: 140 μm) with the PS dissolved in sodium hyaluronate and a transparent needle body (height: 660 μm) prepared from 15 % (w/w) PVA with a transparency of 98.7 %–99.96 %. This MN could markedly raise the incident fluxes via reducing the light scattering and absorption occurring in the stratum corneum, and lower the therapeutic light irradiance by 40 % (from 100 mW cm^{-2} to 60 mW cm^{-2}) to achieve a comparable incident flux beneath the stratum corneum [29]. In another investigation on the phototherapy-immunomodulation treatment of psoriasis (Fig. 8a), a similar two-segment MN consisting a transparent body layer made from poly(methyl methacrylate) (PMMA) and a less transparent drug layer was fabricated (Fig. 8b), and it was shown to enhance the light transmittance (Fig. 8c–e) and the drug to subcutaneous tissue (Fig. 8f). Such a design could maintain up to 80 % of initial light power even at 500 μm beneath the skin (160 % increase compared with the control) to increase the efficacy of both PDT and PTT against psoriasis [143].

4.2.3. *Compact integrated LED in local device enables portable and on-demand PDT*

To enable localized, on-demand light emission directly at the target tissue site, miniaturized electroluminescent modules can be integrated onto light-guiding MNs. This embedded design eliminates reliance on external light sources, improving treatment portability, precision, and spatiotemporal control over therapeutic activation. For example, an all-in-one MN device [2 cm (L) × 1.7 cm (W) × 1.2 cm (H), weighing 3.6 g] powered by battery and controlled through Bluetooth® wireless link was developed for point-of-care PDT therapy (Fig. 9), which was far smaller than the typical clinical used light source instrument [>48.5 cm (L), 22 cm (W), 40.5 cm (H), >19 kg in weight]. On the light-guiding MNs, other four layers are assembled from bottom to top, including a light emitting diode (LED) as the light source, a graphene membrane as heat dissipating component, a control module enabling remotely stimulate LED to emit therapeutic light, and a lithium battery

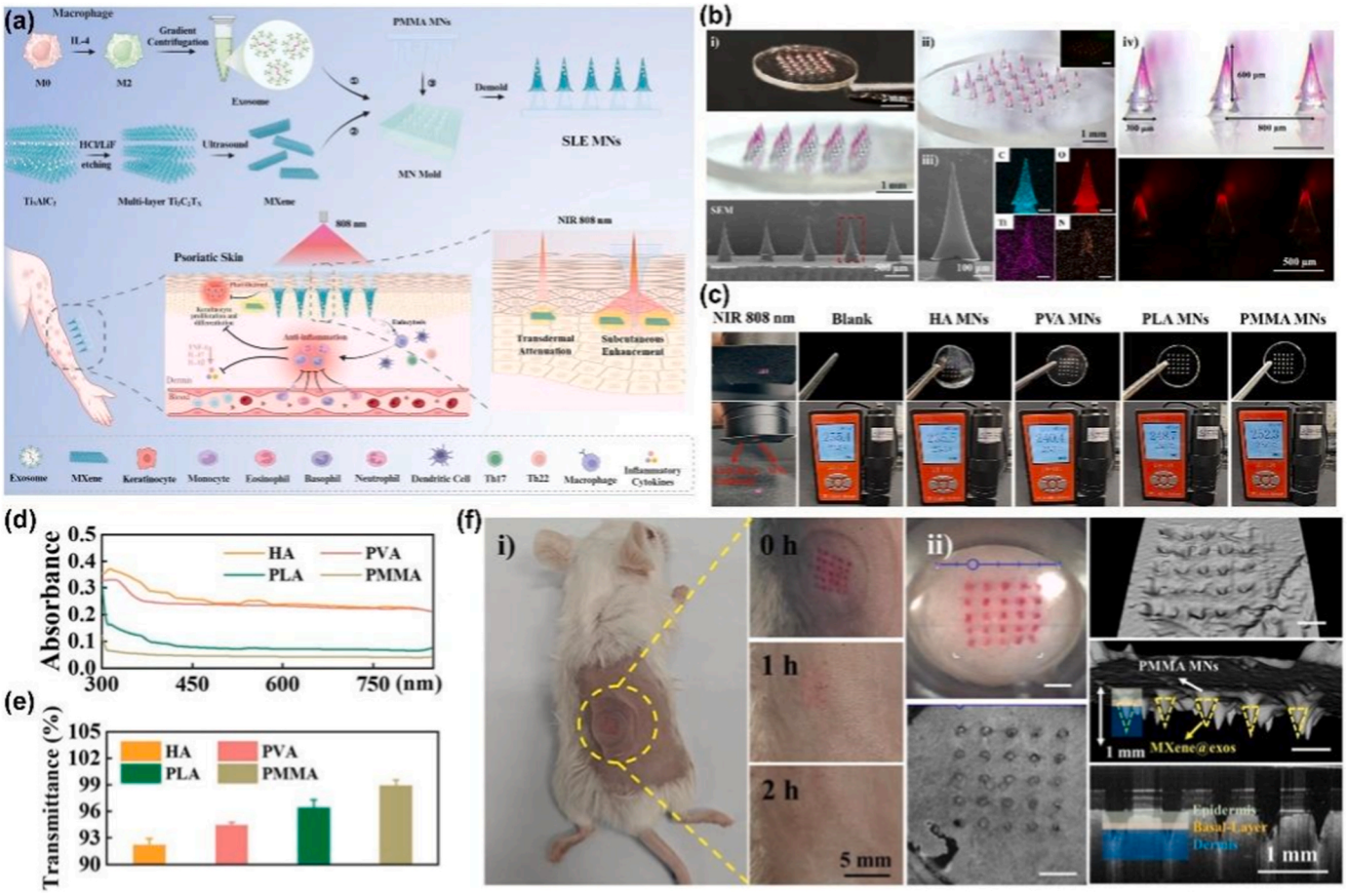

Fig. 8. Two-segment MN for the phototherapy-immunomodulation treatment of psoriasis, including (a) Schematic diagram of the MN preparation and its application the treatment of immune-related psoriasis, (b) morphology and elemental distribution of the MN, (c) 808 nm NIR transmittance of MNs made from various materials, (d) light absorbance of MNs, (e) transmittance of MNs at 808 nm, and (f) OCT images of the MN penetration and subdermal insertion. Copied with permission [143]. Copyright 2025, ACS.

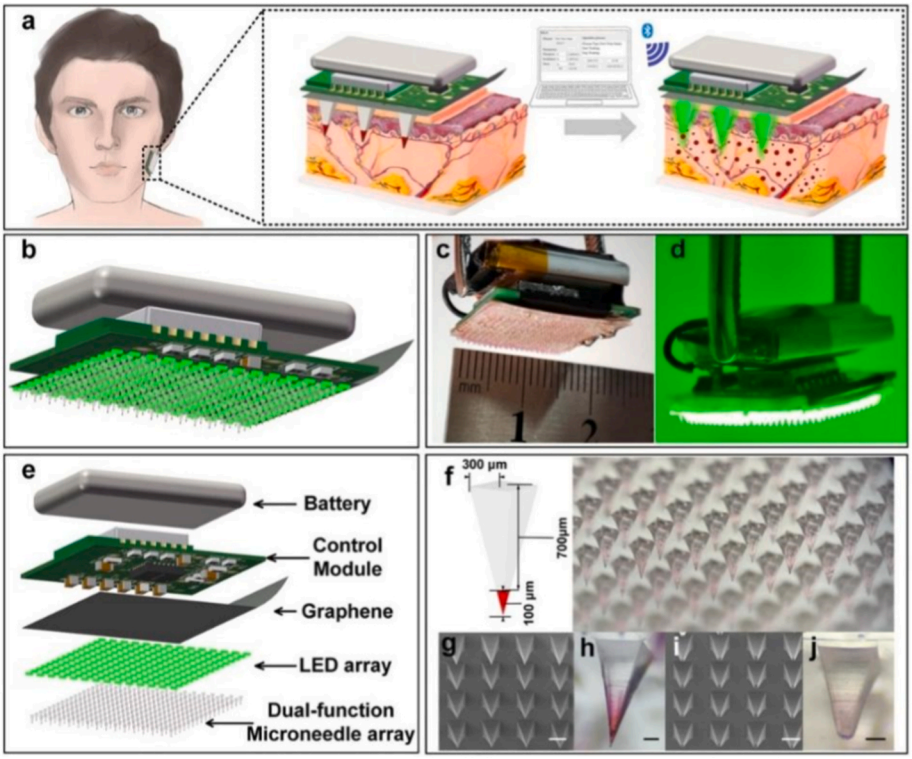

Fig. 9. Application of the all-in-one MN device to treat superficial skin diseases, including (a) the application scheme, (b) the schematic diagram of the MN, (c) the photograph of the MN, (d) the emitting therapeutic light from the MN at 525 nm, (e) exploded view of the MN, (f) the schematic diagram of the single needle, (g) SEM of the MN (scale bar: 300 μm), (h) photograph of a single MN (scale bar: 100 μm), (i) SEM of MNs after tips dissolved (scale bar: 300 μm), and (j) photograph of a single PVA light-guide (scale bar: 100 μm). Copied with permission [144]. Copyright 2024, Springer.

providing power for the device [144]. Alternatively, small LED chips could be assembled and fixed onto the MN array with the aid of a flexible bandage, and then triggered by electromagnetic induction for wireless illumination to optically activate the PS [145].

To enable multi-wavelength therapeutic adaptability in PDT, a dual wavelength microLED system can be introduced to the above system. The device utilizes two frequency-matched resonant circuits to enable independent, interference-free activation of connected microLEDs via resonant inductive coupling, allowing the light emitted at different wavelengths to be emitted independently. Such dual-wavelength emission modules could be employed to sequentially trigger the release of the PS from nanocarriers prepared from light-responsive polymers (e.g., 405 nm for photolysis of PEG45-b-PNBMA30) and activate the PS to generate the ROS (e.g., 660 nm for Rose Bengal lactone as the PS) [146].

However, conventional light sources like LED still have their limitations, such as the difficulty in fitting the human body and patient discomfort during the long-term treatment. Alternating current electroluminescence (ACEL) has emerged as an energy-efficient, flexible light source for biomedical applications due to its low power consumption, mechanical adaptability, and compatibility with large-area fabrication. Meanwhile, triboelectric nanogenerators (TENGs) offer a sustainable solution for self-powered systems by harvesting biomechanical energy (e.g., body motion) into alternating current electricity [147]. For example, a wearable, self-powered metronomic PDT (mPDT) platform was developed using a fully flexible ACEL module with a ZnS:Cu, Al/PDMS emissive layer sandwiched between conductive hydrogel electrodes, one loaded with PS rose bengal (RB). Driven by an origami-inspired TENG that harvests biomechanical energy (e.g., human motion), the system generates pulsed green electroluminescence to activate rose bengal for localized $^1O_2$ production to eradicate wound multidrug-resistant bacteria infection [148].

4.2.4. *Multifunctional materials leverage single-wavelength PDT/PTT synergy to enhance therapeutic efficacy*

The combination of PDT and PTT has gained significant interest in recent years, particularly with the advent of multimodal nanoplatforms capable of co-delivering both photodynamic and photothermal agents [149,150]. This strategy has a potent synergistic effect through dual complementary pathways whereby the PDT-generated ROS can down-regulate heat shock proteins to sensitize cells towards PTT, and the PTT-induced hyperthermia can improve tissue oxygenation and molecular diffusion to mitigate the oxygen dependence of PDT [151]. In addition, both of them can boost the efficacy of the immunotherapy by inducing the immunogenic cell death (ICD) to reshape the tumor immune microenvironment [152–154]. Especially, the PDT/PTT combination can overcome the immunosuppressive barrier via a coordinated cascade process [155,156]. Their synergistic cytotoxic effect initiates the release of tumor associated antigens (TAAs) and inflammatory cytokines, which in turn triggers an adaptive immune response and amplifies ICD. This process leads to the further release of damage-associated molecular patterns (DAMPs), activating antigen-presenting cells (APCs) to secrete proinflammatory cytokines and thereby trigger effective immune response. The ROS-induced cellular damage could relieve immunosuppression and stimulate T cells and natural killer (NK) cells, thereby boosting anti-tumor effect [155]. Therefore, the combined PDT and PTT strategy presents a highly promising avenue for further therapeutic development.

Due to the distinct wavelengths for activation of PSs (600–800 nm, 630 nm, and 660 nm used mostly) and photothermal agents (650–1100 nm, 808 nm used mostly), dual-wavelength strategy is often utilized to ensure efficient activation of both agents and maximize their respective functions [157,158]. However, this approach faces limitations including technical complexity, the requirement of dual light sources, and potential energy interference from overlapping absorption spectra. The unification of PDT and PTT under a single-wavelength

platform represents a transformative advancement in light therapy, addressing critical limitations of conventional dual-wavelength phototherapeutic approaches.

Indocyanine Green (ICG), a clinically approved NIR fluorescent dye, exhibits dual functionality for both PDT and PTT at a single wavelength (typically 808 nm) [158–160]. It can also be synergistically combined with other photothermal agents (e.g., polydopamine nanoparticles) to harness complementary mechanisms of PDT and PTT at a shared wavelength (e.g., 808 nm) [161]. Considering the poor permeability into deep skin, such cyanine dye with strong mitochondrial selectivity can be formulated into nanoparticles (such as ethosomes) to achieve effective transdermal PDT/PTT. The incorporation of the dye into such nano-carriers would also lead to an aggregation-induced emission (AIE) enhancement to avoid luminescence quenching. This system was found effective in the treatment of hypertrophic scars, via promoting fibroblast apoptosis and collagen remodeling [162].

Recent advances in nanotechnology have driven the development of composite nanomaterials capable of simultaneously enabling PDT and PTT under a single excitation wavelength. For example, the polydopamine/Ce6/black phosphorus nanosheets can provide both PDT and PTT effects at the wavelength of 660 nm [163]. By precisely tuning the localized surface plasmon resonance (LSPR) of photothermal noble metal-based nanomaterials (e.g., graphene-gold nanostar hybrids) to align with the excitation wavelength of the PS Ce6 (e.g., 660 nm) and simultaneously serving as a carrier, both the absorption band of the nanomaterial and the activation wavelength of Ce6 can be synergistically matched. This dual alignment enables simultaneous heat generation and singlet oxygen production at the identical wavelength [164]. The PS brominated hemicyanine can be loaded into the photothermal Ag_2S quantum dots, and achieve both effects at 640 nm irradiation [165].

However, conventional composite materials for combined PDT/PTT therapy have historically relied on a simplistic “two-in-one” design via mechanical blending or physical encapsulation. While functional, this approach suffers from inherent drawbacks like multi-step synthesis, weak interfacial coupling between components, and premature PS leakage or photothermal agent aggregation, ultimately compromising therapeutic synergy and reproducibility. Recent advances in MOF-based nanomedicine have spotlighted “all-in-one” platforms for single-wavelength synergetic PDT/PTT. For example, Fu et al. developed an iron-doped zinc-centered organic framework mesoporous carbon derivative (Fex-Zn-NCT) with strong absorption within the range of 600–1000 nm wavelength. Under 808 nm laser, it exhibited excellent photothermal conversion ability ($\eta \approx 81.3$ %), as well as strong $^1O_2$ generation capability ($\Phi \approx 0.0041$, ICG as reference) [166]. Such a design paves the way for scalable, patient-friendly phototherapy systems with extensive applicability and adaptability while reducing healthcare burden and costs.

4.3. Translational barriers and implications

The material-based strategies previously discussed, although innovative, present distinct challenges that must be addressed to facilitate their clinical translation. In the case of OCAs, significant limitations include the potential for skin irritation, the temporary nature of the clearing effect necessitating repeated applications, and the challenge of achieving uniform penetration sufficient for treating deep-seated lesions [167]. MN-based light guides face issues related to mechanical strength, such as ensuring painless penetration without fracture, as well as potential inflammatory responses due to the materials embedded in the skin. Although compact integrated LED devices provide excellent portability, their therapeutic efficacy is limited by their restricted power output and the need for precise control over irradiance and thermal effects at the target site [168]. The advancement of multifunctional materials for the synergistic application of PDT/PTT is hindered by the complex synthesis processes necessary to optimize the properties of both therapeutic modalities. Additionally, challenges arise from the risk of uncontrolled heat diffusion, which may lead to collateral tissue damage, and the difficulty of achieving a precisely synchronized therapeutic effect at a single wavelength [169]. Importantly, these strategies must address critical safety concerns, including the long-term biocompatibility and biodegradation pathways of novel materials, potential immune responses to foreign components, and the need for precise spatial-temporal control of thermal energy in PTT to prevent adverse effects such as scarring or hyperpigmentation, particularly in cosmetically sensitive regions such as the skin.

Future research directions are anticipated to concentrate on the development of more intelligent, integrated, and safety-oriented systems. It is expected that composite MNs will emerge, integrating light-guiding capabilities with biodegradable polymers and encapsulated OCAs to enhance light delivery. The forthcoming generation of wearable LED devices is likely to feature real-time dosimetry and thermal feedback mechanisms that automatically adjust parameters to ensure both safety and efficacy. A significant overarching trend will be the convergence of these strategies [170,171]. For instance, employing MNs for OCA delivery and implantable biodegradable light guides, in conjunction with a topically applied photosensitizer, all regulated by a wearable smart LED patch. Ultimately, the successful translation of these advanced material-based approaches will depend on comprehensive safety assessments and a holistic design philosophy that emphasizes patient-specific applicability, minimal invasiveness, and robust control.

5. Advanced PS formulations from clinical trials to market

Despite remarkable progress in PDT, translating advanced PS formulations from laboratory innovations into clinical investigation and, ultimately, commercial products remain a persistent challenge, with only a handful have reached the global market for practical use. These include injectable agents such as porfimer sodium (Photofrin®) and talaporfin (Laserphyrin®), both as lyophilized powders for injection; hematoporphyrin (HiPorfin®) and temoporfin (Foscan®) as solutions for injection; and agents for intravenous infusion like padoporfin (Tookad®), chlorin derivatives (Radachlorin®), and liposomal verteporfin (Visudyne®) as lyophilized powder, as solutions for infusion. The landscape is further broadened by targeted biologics such as cetuximab sarotalocan sodium (Akalux®), an antibody-dye conjugate for infusion, which has received its first global approval by Japan in 2020, as a pioneering photoimmunotherapy agent [172].

By contrast to the above systemically administered PSs, the clinical translation of topically applied PSs has been more constrained. The cornerstone of topical PDT is the use of prodrugs, primarily 5-ALA and its ester derivative methyl aminolevulinate (MAL). They are commercially formulated for direct application to the skin: ALA as a topical solution (Levulan® Kerastick®) and, more recently, in an enhanced nanoemulsion gel (BF-200 ALA/Ameluz®), while MAL is available as a cream (Metvix®/Metvixia®) [15]. Beyond the barriers detailed herein, this translational gap is further driven by a spectrum of translational challenges, including the intrinsic complexity of the therapeutic system, manufacturing scalability constraints, variable in vivo performance, insufficient long-term safety evidence, and hurdles in achieving seamless integration with medical devices such as light source and MNs.

To assess the current status and emerging trends of PSs in clinical development, we conducted a search on ClinicalTrials.gov. Using “photodynamic therapy” as a key term, this search identified 95 active clinical trials for PS formulations, of which those focusing on dermal applications are summarized in Table 3. These investigated strategies follow two complementary pathways: developing novel PSs and repurposing existing commercialized formulations. They are realized through several key approaches including combination with other treatment modalities, exploration of new therapeutic indications, optimization of light sources and dosimetry parameters, development of personalized treatment regimens, and investigation of PDT-induced immunity as well

Table 3
Overview of active PS clinical trials registered on ClinicalTrials.gov.

PSs	Dosage form	Delivery route	Light	Target condition	Phase	Study objective
ALA	O/W emulsion combined with hydrogel dressing	Topical	Red	Chronic wounds	N/A	To investigate the clinical effectiveness of topical ALA-PDT combined with a hydrogel dressing towards chronic wounds.
Chlorin-e6	N/S	Topical	Red	Moderate to severe acne	II	To evaluate the efficacy, safety and tolerability of chlorin-e6 based PDT towards moderate to severe acne.
HAL ALA MAL	Cream Nanoemulsion gel (BF-200) Cream (Metvixia®)	Topical	N/S	Superficial basal cell cancer	I&II	To compare efficacy of different PSs based on fluorescence measurement.
ALA	Solution (Levulan® Kerastick®) combined with oral sonidegib	Topical	Blue (BLU-U Model 4170E)	Multiple basal cell carcinoma lesions	I	To test the therapeutic outcome of the PDT combined with sonidegib
ALA	Solution (Levulan® Kerastick®)	Topical	Red (630 nm)	Dermal neurofibromas	II	To assess the therapeutic effect by determining the time to disease progression and analyzing tumor growth rates.
ALA	Solution (Levulan® Kerastick®)	Topical	Blue	Actinic keratosis	N/A	To compare the feasibility of two ALA incubation times (0 vs. 1 h).
Toluidine blue	Gel combined with ciclopirox 8 %	Topical	Red (635 nm)	Onychomycosis in diabetes	N/A	To evaluate the effectiveness and safety of PDT combined with conventional antifungal therapy.
Methylene blue	Solution	Local intracavitary instillation	Red (665 nm)	Deep tissue abscesses	II	To evaluate the efficacy of methylene blue based PDT during percutaneous drainage for deep tissue abscess disinfection.
Methylene blue	Solution	Local intracavitary instillation	Red (665 nm)	Breast abscesses	II	To evaluate the efficacy of methylene blue based PDT during percutaneous drainage for breast disinfection.
Methylene blue	Solution	Topical	Red (660 nm)	Wound and tissue repair in the diabetic foot	N/A	To evaluate the impact of antimicrobial photodynamic therapy (aPDT) on wound quality and tissue repair in diabetic foot ulcers using the Bates-Jensen scale.
MAL	Cream	Topical	Red (630 nm, half and full dose)	Actinic keratoses	N/A	To compare the efficacy and tolerance of full-dose versus half-dose red light PDT, and to analyze their biomolecular-level effects.
Methylene Blue	Solution combined with 40 % urea cream	Topical	LED (different doses)	Onychomycosis	N/A	To determine the optimal light dose and treatment frequency of home-based PDT for onychomycosis.
ALA	Nanoemulsion gel (BF-200, Ameluz®)	Topical	Red (RhodoLED-XL®)	Facial cutaneous squamous cell carcinoma	II	To test the safety and effectiveness to treat early form of cancer cells found in the upper skin layer of the face.
Zn(II) Phthalocyanine	Gel	Topical	Red (630 nm)	Moderate-to-severe acne vulgaris	N/A	To evaluate the safety, tolerability, and efficacy of a novel zinc phthalocyanine-based PDT for moderate-to-severe acne vulgaris.
ALA	Solution (Reformulated Levulan® Kerastick®)	Topical	Blue (BLU-U® model 4170E)	Actinic keratosis on upper extremities	III	To evaluate the efficacy and safety of a reformulated ALA-PDT for the field-directed treatment of actinic keratosis on the upper extremities.
ALA	Solution (Reformulated Levulan® Kerastick®)	Topical	Blue (BLU-U® model 4170E)	Actinic keratosis on face and scalp	III	To evaluate the efficacy and safety of a reformulated ALA-PDT for field-directed treatment of actinic keratosis on the face or bald scalp.
ALA	Nanoemulsion gel (BF-200, Ameluz®)	Topical	Red (RhodoLED®)	Superficial basal cell carcinoma	III	To evaluate the safety and efficacy of BF-200 ALA and BF-RhodoLED® in the treatment of superficial basal cell carcinoma (sBCC) with PDT.
ALA	Nanoemulsion gel (BF-200, Ameluz®)	Topical	Red (RhodoLED®)	Moderate to severe acne vulgaris	II	To evaluate the safety and efficacy of BF-200 ALA and BF-RhodoLED® in the treatment of moderate to severe acne vulgaris with PDT.
ALA	Nanoemulsion gel (BF-200, Ameluz®)	Topical	Red LED (RhodoLED®)	Actinic keratosis (AK) on the extremities and neck/trunk	III	To evaluate the safety, tolerability and efficacy of BF-200 ALA in the field-directed treatment of actinic keratosis on the extremities and neck/trunk with PDT (PDT) using a RhodoLED lamp.
ALA	Solution (Levulan® Kerastick®)	Topical	Red	Actinic keratoses	II	To test imaging techniques to monitor photosensitizer and sO_2 levels during PDT of actinic keratoses.
ALA	N/S	Topical	Blue	Nonmelanoma skin cancer	N/A	To test effects of vitamin D on immune microenvironment of nonmelanoma skin cancer after PDT.
ALA	N/S	Topical	Blue	Basal cell carcinoma	II	To better understand the immune response to basal cell carcinoma treated with PDT.
ALA	Nanoemulsion gel (BF-200, Ameluz®)	Topical	Broad band light	Actinic keratoses and photodamage	I	To provide a treatment of both actinic keratoses and photodamage within one ALA based PDT using broad band light.

Note for this table: Data are current as of January 1, 2026. The drug label marked as Levulan® is uniformly standardized as Levulan® Kerastick®; the formulation marked Ameluz® is consistently referred to as "Nanoemulsion gel (BF-200, Ameluz®)". Abbreviation: aminolevulinic acid, ALA; hexylaminolevulinate, HAL; methylaminolevulinate: MAL; NA: not available; N/S: not specified.

as singlet oxygen/PpIX imaging. Topical application is the primary route of administration in dermatological PDT, with local injection also employed. Despite considerable promise in preclinical studies, the entry of advanced material-based carriers for PS dermal delivery into clinical trials has been exceptionally scarce. This huge gap not only reflects the formidable challenges in biocompatibility, scalable manufacturing, and regulatory approval but also positions them as a compelling yet long-term frontier for innovation in PDT.

6. Conclusion and further perspective

PDT has transformed dermatologic care by offering a minimally invasive, targeted treatment for various skin conditions, from precancerous lesions to inflammatory disorders. By using light-activated PSs to create localized oxidative stress, it selectively destroys tissue while maintaining cosmetic appearance, especially in sensitive areas like the face and scalp. Despite challenges in clinical application, such as controlling PS delivery and photon efficiency, along with persistent concerns regarding the biocompatibility, in vivo biological fate, and long-term toxicity of materials employed in PDT systems, advancements in materials, bioengineering, and optics are enhancing its therapeutic potential.

Emerging paradigms in PDT now incorporate theranostic platforms that seamlessly integrate real-time diagnostic imaging with adaptive light delivery or controlled PS release. This integration facilitates dynamic treatment modifications based on biomarker or biosignal feedback. Concurrently, synergistic approaches that combine PDT with immunomodulatory agents are enhancing therapeutic efficacy and inducing systemic immune responses. The co-development of device and drug technologies signifies a transformative advancement in PDT, wherein light delivery systems and PS formulations are designed as synergistic, interdependent elements rather than as separate technologies. This integrated platform represents a shift towards "intelligent PDT ecosystems," where devices not only deliver light but also actively influence drug pharmacokinetics. Additionally, the application of artificial intelligence in personalizing PDT protocols optimizes treatment by aligning parameters with individual skin profiles and lesion characteristics, thereby minimizing side effects and enhancing therapeutic precision across diverse patient populations.

The transition of next-generation PDT from experimental innovation to a standard clinical practice necessitates a comprehensive integration of multidisciplinary expertise, scalable manufacturing frameworks, and patient-centered design. Although substantial progress has been made in overcoming biological and technical challenges, the ultimate success of PDT depends on effectively bridging the gap between laboratory breakthroughs and real-world application. Future efforts must prioritize clinical translation strategies that address cost-effectiveness, reproducibility, regulatory harmonization, and key biosafety considerations, such as assessing material biocompatibility, elucidating in vivo biological fate, mitigating long-term toxicity risks, and addressing other associated clinical translation obstacles. By fostering collaborations among material scientists, clinicians, and industrial partners, the field can expedite the development of adaptive PDT platforms tailored to diverse dermatological needs. As these innovations converge, PDT is poised to transition from a supplementary therapy to a first-line modality, offering precise, accessible, and aesthetically conscious solutions that redefine standards of care in global dermatology.

CRediT authorship contribution statement

Xun Feng: Funding acquisition, Writing – original draft. **Hua Fan:** Writing – original draft. **Lubin Zhou:** Writing – original draft. **Zhilong Zhao:** Data curation. **Mu Yang:** Funding acquisition, Writing – review & editing. **Xinxing Sun:** Writing – review & editing. **Yang Chen:** Conceptualization, Data curation, Writing – review & editing.

Declaration of competing interest

The authors declare that they have no known competing financial interests or personal relationships that could have appeared to influence the work reported in this paper.

Acknowledgment

This work was supported by the Joint Fund of Natural Science Foundation of Liaoning Province (2023-MSLH-296) and Young Talent Innovation and Entrepreneurship Program of Liaoning Inspection Examination & Certification Centre (SC202501).

Data availability

No data was used for the research described in the article.

References

[1] X. Cheng, J. Gao, Y. Ding, Y. Lu, Q. Wei, D. Cui, J. Fan, X. Li, E. Zhu, Y. Lu, Multifunctional liposome: a powerful theranostic nano-platform enhancing photodynamic therapy, Adv. Sci. 8 (2021) 2100876, https://doi.org/10.1002/advs.202100876.

[2] M. Li, J. Xiong, Y. Zhang, L. Yu, L. Yue, C. Yoon, Y. Kim, Y. Zhou, X. Chen, Y. Xu, New guidelines and definitions for type I photodynamic therapy, Chem. Soc. Rev. 54 (2025) 7025–7057, https://doi.org/10.1039/d1cs01079d.

[3] M.-T. IS, D. LD, I. NM, Features of third generation photosensitizers used in anticancer photodynamic therapy, Photodiagnosis Photodyn. Ther. 34 (2021) 102091, https://doi.org/10.1016/j.pdpdt.2020.102091.

[4] M. Kolarikova, B. Hosikova, H. Dilenko, K. Barton-Tomankova, L. Valkova, R. Bajgar, L. Malina, H. Kolarova, Photodynamic therapy: innovative approaches for antibacterial and anticancer treatments, Med. Res. Rev. 43 (2023) 717–774, https://doi.org/10.1002/med.21935.

[5] N. Dragicevic, J. Predic-Atkinson, B. Nikolic, S.B. Pajovic, S. Ivkovic, M. Adzic, Nanocarriers in topical photodynamic therapy, Expet Opin. Drug Deliv. 21 (2) (2024) 279–307, https://doi.org/10.1080/17425247.2024.2318460.

[6] C. Morton, R.M. Szeimies, N. Basset-Séguin, P. Calzavara-Pinton, Y. Gilaberte, M. Haedersdal, G. Hofbauer, R. Hunger, S. Karrer, S. Piaserico, European dermatology forum guidelines on topical photodynamic therapy 2019 part 2: emerging indications-field cancerization, photorejuvenation and inflammatory/infective dermatoses, J. Eur. Acad. Dermatol. Venereol. 34 (2020) 17–29, https://doi.org/10.1111/jdv.16044.

[7] M. Kim, H.Y. Jung, H.J. Park, Topical PDT in the treatment of benign skin diseases: principles and new applications, Int. J. Mol. Sci. 16 (2015) 23259–23278, https://doi.org/10.3390/ijms161023259.

[8] Q. Wang, N. Chen, M. Li, S. Yao, X. Sun, X. Feng, Y. Chen, Light-related activities of metal-based nanoparticles and their implications on dermatological treatment, Drug Deliv. Transl. Res. 13 (2023) 386–399, https://doi.org/10.1007/s13346-022-01216-4.

[9] S. Kwiatkowski, B. Knap, D. Przystupski, J. Saczko, E. Kędzierska, K. Knap-Czop, J. Kotlińska, O. Michel, K. Kotowski, J. Kulbacka, Photodynamic therapy–mechanisms, photosensitizers and combinations, Biomed. Pharmacother. 106 (2018) 1098–1107, https://doi.org/10.1016/j.biopha.2018.07.049.

[10] L.R. Braathen, R.-M. Szeimies, N. Basset-Seguin, R. Bissonnette, P. Foley, D. Pariser, R. Roelandts, A.-M. Wennberg, C.A. Morton, Guidelines on the use of photodynamic therapy for nonmelanoma skin cancer: an international consensus, J. Am. Acad. Dermatol. 56 (2007) 125–143, https://doi.org/10.1016/j.jaad.2006.06.006.

[11] R. Bissonette, A. Bergeron, Y. Liu, Large surface photodynamic therapy with aminolevulinic acid: treatment of actinic keratoses and beyond, J. Drugs Dermatol. JDD 3 (1 Suppl) (2004) S26–S31.

[12] R. Tian, X. Wang, Y. Li, L. Zhang, X. Wen, Application of microneedling in photodynamic therapy: a systematic review, Photodiagnosis Photodyn. Ther. 46 (2024) 104016, https://doi.org/10.1016/j.pdpdt.2024.104016.

[13] M. Champeau, S. Vignoud, L. Mortier, S. Mordon, Photodynamic therapy for skin cancer: how to enhance drug penetration? J. Photochem. Photobiol., B 197 (2019) 111544 https://doi.org/10.1016/j.jphotobiol.2019.

[14] J. Ruan, S. Liao, J. Tang, Y. Ou, X. Hu, J. Li, The effect of skin diffusion kinetics of isopropyl ester permeation enhancers on drug permeation: role of lateral spread and penetration characteristics, Int. J. Pharm. 660 (2024) 124297, https://doi.org/10.1016/j.ijpharm.2024.124297.

[15] T. Wu, W.-T. Dou, C. Yang, L. Zhou, F. Wang, L. He, X. Qian, L. Xu, Small molecule photosensitizers: paving the way for improved photodynamic therapy in dermatology, Coord. Chem. Rev. 541 (2025) 216839, https://doi.org/10.1016/j.ccr.2025.216839.

[16] G. Tan, Q. Zhong, J. Zhang, P. He, X. Zhao, G. Miao, Y. Xu, X. Wang, A general strategy towards activatable nanophotosensitizer for phototoxicity-free photodynamic therapy, Theranostics 15 (3) (2025) 943, https://doi.org/10.7150/thno.100597.

[17] D. Mijaljica, J.P. Townley, F. Spada, I.P. Harrison, The heterogeneity and complexity of skin surface lipids in human skin health and disease, Prog. Lipid Res. 93 (2024) 101264, https://doi.org/10.1016/j.plipres.2023.101264.
[18] C.P.H. Reinehr, L. de Mattos Milman, V. Campos, Understanding skin and drug delivery, in: C.L.P.V. Kalil, V. Campos (Eds.), Drug Delivery in Dermatology: Fundamental and Practical Applications, Springer, 2021, pp. 1–10, https://doi.org/10.1007/978-3-030-81807-4_1.
[19] J. Ruan, C. Liu, H. Song, T. Zhong, P. Quan, L. Fang, A skin pharmacokinetics study of permeation enhancers: the root cause of dynamic enhancement effect on in vivo drug permeation, Eur. J. Pharm. Biopharm. 184 (2023) 170–180, https://doi.org/10.1016/j.ejpb.2023.01.022.
[20] S. Mitragotri, Modeling skin permeability to hydrophilic and hydrophobic solutes based on four permeation pathways, J. Contr. Release 86 (2003) 69–92, https://doi.org/10.1016/s0168-3659(02)00321-8.
[21] S. Kezic, J.B. Nielsen, Absorption of chemicals through compromised skin, Int. Arch. Occup. Environ. Health 82 (2009) 677–688, https://doi.org/10.1007/s00420-009-0405-x.
[22] G.B. Kasting, M.A. Miller, T.D. LaCount, J. Jaworska, A composite model for the transport of hydrophilic and lipophilic compounds across the skin: steady-state behavior, J. Pharmacol. Sci. 108 (2019) 337–349, https://doi.org/10.1016/j.xphs.2018.09.007.
[23] R.S. Ingrole, E. Azizoglu, M. Dul, J.C. Birchall, H.S. Gill, M.R. Prausnitz, Trends of microneedle technology in the scientific literature, patents, clinical trials and internet activity, Biomaterials 267 (2021) 120491, https://doi.org/10.1016/j.biomaterials.2020.120491.
[24] Y. Chen, X. Feng, S. Meng, Site-specific drug delivery in the skin for the localized treatment of skin diseases, Expet Opin. Drug Deliv. 16 (2019) 847–867, https://doi.org/10.1080/17425247.
[25] Z. Le, J. Yu, Y.J. Quek, B. Bai, X. Li, Y. Shou, B. Myint, C. Xu, A. Tay, Design principles of microneedles for drug delivery and sampling applications, Mater. Today 63 (2023) 137–169, https://doi.org/10.1016/j.mattod.2022.10.025.
[26] J. Zhuang, F. Rao, D. Wu, Y. Huang, H. Xu, W. Gao, J. Zhang, J. Sun, Study on the fabrication and characterization of tip-loaded dissolving microneedles for transdermal drug delivery, Eur. J. Pharm. Biopharm. 157 (2020) 66–73, https://doi.org/10.1016/j.ejpb.2020.10.002.
[27] Y. Yu, W. Li, Q. Li, W. Liu, S. Zhang, X. Zhang, J. Liang, Review of microneedle technology for targeted therapeutics in vitiligo: design principles, application prospects, Drug Des. Dev. Ther. (2024) 4901–4914, https://doi.org/10.2147/DDDT.
[28] X. Zhao, X. Li, P. Zhang, J. Du, Y. Wang, Tip-loaded fast-dissolving microneedle patches for photodynamic therapy of subcutaneous tumor, J. Contr. Release 286 (2018) 201–209, https://doi.org/10.1016/j.jconrel.2018.07.038.
[29] H. Zhao, X. Wang, Z. Geng, N. Liang, Q. Li, X. Hu, Z. Wei, Dual-function microneedle array for efficient photodynamic therapy with transdermal co-delivered light and photosensitizers, Lab Chip 22 (2022) 4521–4530, https://doi.org/10.1039/d2lc00505k.
[30] G. He, Y. Li, M.R. Younis, L.-H. Fu, T. He, S. Lei, J. Lin, P. Huang, Synthetic biology-instructed transdermal microneedle patch for traceable photodynamic therapy, Nat. Commun. 13 (2022) 6238, https://doi.org/10.1038/s41467-022-33837-1.
[31] B. Zheng, Q. Li, L. Fang, X. Cai, Y. Liu, Y. Duo, B. Li, Z. Wu, B. Shen, Y. Bai, Microorganism microneedle micro-engine depth drug delivery, Nat. Commun. 15 (2024) 8947, https://doi.org/10.1038/s41467-024-53280-8.
[32] Z. Li, Z. Zhou, Y. Wang, J. Wang, L. Zhou, H.-B. Cheng, J. Yoon, Activatable nano-photosensitizers for precise photodynamic cancer therapy, Coord. Chem. Rev. 493 (2023) 215324, https://doi.org/10.1016/j.ccr.2023.215324.
[33] Y. Chen, N. Chen, X. Feng, The role of internal and external stimuli in the rational design of skin-specific drug delivery systems, Int. J. Pharm. 592 (2021) 120081, https://doi.org/10.1016/j.ijpharm.2020.120081.
[34] Q. Ding, L. Ding, C. Xiang, C. Li, E. Kim, C. Yoon, H. Wang, M. Gu, P. Zhang, L. Wang, pH-responsive AIE photosensitizers for enhanced antibacterial therapy, Angew Chem. Int. Ed. Engl. 64 (2025) e202506505, https://doi.org/10.1002/anie.202506505.
[35] H. Yang, Y. Yang, Z. Zhu, P. Chen, J. Gao, Y. Lin, Q. Wang, F. Hu, Glutathione-depleting photosensitizers for tumor-specific imaging and pyroptosis-driven photodynamic therapy, Theranostics 16 (2026) 1818–1832, https://doi.org/10.7150/thno.124154.
[36] E. Nestoros, A. Sharma, E. Kim, J.S. Kim, M. Vendrell, Smart molecular designs and applications of activatable organic photosensitizers, Nat. Rev. Chem 9 (2025) 46–60, https://doi.org/10.1038/s41570-024-00662-7.
[37] F. Liu, Z. Cheng, H. Yi, NIR light-activatable dissolving microneedle system for melanoma ablation enabled by a combination of ROS-responsive chemotherapy and phototherapy, J. Nanobiotechnol. 21 (2023) 61, https://doi.org/10.1186/s12951-023-01815-4.
[38] Y. Huang, H. Lai, J. Jiang, X. Xu, Z. Zeng, L. Ren, Q. Liu, M. Chen, T. Zhang, X. Ding, pH-activatable oxidative stress amplifying dissolving microneedles for combined chemo-photodynamic therapy of melanoma, Asian J. Pharm. Sci. 17 (2022) 679–696, https://doi.org/10.1016/j.ajps.2022.08.003.
[39] A. Han, C. Liu, Q. Wu, Z. Gong, M. Liu, B. Xu, X. Su, External physical field-responsive nanocomposite hydrogels for wound healing applications, Adv. Nanocomp. 2 (2025) 32–58, https://doi.org/10.1016/j.adna.2024.11.002.
[40] L.-K. Zhang, S. Du, X. Wang, Y. Jiao, L. Yin, Y. Zhang, Y.-Q. Guan, Bacterial cellulose based composites enhanced transdermal drug targeting for breast cancer treatment, Chem. Eng. J. 370 (2019) 749–759, https://doi.org/10.1016/j.cej.2019.03.216.
[41] H. Wang, R. Cai, S. Wang, Y. Yang, T. Sheng, W. Zhang, S. Wang, J. You, Z. Lu, K. Ji, A wearable transdermal device for on-demand drug delivery, Matter 8 (2025), https://doi.org/10.1016/j.matt.2025.102040.
[42] S. Wang, C. Yang, W. Zhang, S. Zhao, J. You, R. Cai, H. Wang, Y. Bao, Y. Zhang, J. Zhang, Glucose-responsive microneedle patch with high insulin loading capacity for prolonged glycemic control in mice and minipigs, ACS Nano 18 (2024) 26056–26065, https://doi.org/10.1021/acsnano.4c05562.
[43] R. Zhang, Y. Tian, L. Pang, T. Xu, B. Yu, H. Cong, Y. Shen, Wound microenvironment-responsive protein hydrogel drug-loaded system with accelerating healing and antibacterial property, ACS Appl. Mater. Interfaces 14 (2022) 10187–10199, https://doi.org/10.1021/acsami.2c00373.
[44] Y. Sun, X. Jing, Y. Liu, B. Yu, H. Hu, H. Cong, Y. Shen, A chitosan derivative-crosslinked hydrogel with controllable release of polydeoxyribonucleotides for wound treatment, Carbohydr. Polym. 300 (2023) 120298, https://doi.org/10.1016/j.carbpol.2022.120298.
[45] C. Yang, T. Sheng, W. Hou, J. Zhang, L. Cheng, H. Wang, W. Liu, S. Wang, X. Yu, Y. Zhang, Glucose-responsive microneedle patch for closed-loop dual-hormone delivery in mice and pigs, Sci. Adv. 8 (2022), https://doi.org/10.1126/sciadv.add3197 eadd3197.
[46] X. Wang, D. Luo, J.P. Basilion, Photodynamic therapy: targeting cancer biomarkers for the treatment of cancers, Cancers 13 (2021) 2992, https://doi.org/10.3390/cancers13122992.
[47] L. Lin, L. Xiong, Y. Wen, S. Lei, X. Deng, Z. Liu, W. Chen, X. Miao, Active targeting of nano-photosensitizer delivery systems for photodynamic therapy of cancer stem cells, J. Biomed. Nanotechnol. 11 (2015) 531–554, https://doi.org/10.1166/jbn.2015.2090.
[48] L.E. Ibarra, Development of nanosystems for active tumor targeting in photodynamic therapy, Ther. Deliv. 13 (2022) 71–74, https://doi.org/10.4155/tde-2021-0083.
[49] H. Shan, X. Wang, Q. Wei, H. Dai, X. Chen, Enriched photosensitizer for deep-seated-tumor photodynamic therapy, Photonics Res. 12 (2024) 1024–1035, https://doi.org/10.1364/PRJ.515233.
[50] A.A. Sebak, I.E.O. Gomaa, A.N. ElMeshad, M.H. AbdelKader, Targeted photodynamic-induced singlet oxygen production by peptide-conjugated biodegradable nanoparticles for treatment of skin melanoma, Photodiagnosis Photodyn. Ther. 23 (2018) 181–189, https://doi.org/10.1016/j.pdpdt.2018.05.017.
[51] X. Wang, J. Wang, J. Li, H. Huang, X. Sun, Y. Lv, Development and evaluation of hyaluronic acid-based polymeric micelles for targeted delivery of photosensitizer for photodynamic therapy in vitro, J. Drug Deliv. Sci. Technol. 48 (2018) 414–421, https://doi.org/10.1016/j.jddst.2018.10.018.
[52] D. Lei, J. Xin, F. Qin, H. Lan, J. Liu, S. Wang, J. Wang, W. Zeng, C. Yao, Soluble hyaluronic acid microneedle arrays mediated RGD-modified liposome delivery for pain relief during photodynamic therapy by blocking TRPV1, Int. J. Biol. Macromol. 282 (2024) 136952, https://doi.org/10.1016/j.ijbiomac.2024.136952.
[53] C. Naidoo, C.A. Kruger, H. Abrahamse, Targeted photodynamic therapy treatment of in vitro A375 metastatic melanoma cells, Oncotarget 10 (2019) 6079, https://doi.org/10.18632/oncotarget.27221.
[54] J. Yan, T. Gao, Z. Lu, J. Yin, Y. Zhang, R. Pei, Aptamer-targeted photodynamic platforms for tumor therapy, ACS Appl. Mater. Interfaces 13 (2021) 27749–27773, https://doi.org/10.1021/acsami.1c06818.
[55] J. Zhu, L. Peng, S. Jehan, H. Wang, X. Chen, S. Zhao, W. Zhou, Activable photodynamic DNA probe with an "AND" logic gate for precision skin cancer therapy, Research 7 (2024) 295, https://doi.org/10.34133/research.0295.
[56] Y. Hao, Y. Chen, X. He, R. Han, C. Yang, T. Liu, Y. Yang, Q. Liu, Z. Qian, RGD peptide modified platinum nanozyme Co-loaded glutathione-responsive prodrug nanoparticles for enhanced chemo-photodynamic bladder cancer therapy, Biomaterials 293 (2023) 121975, https://doi.org/10.1016/j.biomaterials.2022.121975.
[57] R. Xie, D. Fan, Y. Fang, T. Zhu, H. Li, Y. Yin, X. Liu, Y. Ma, F. Chen, W. Zeng, Dissolving microneedles embedded with photosensitizers for targeted eradication of gram-positive bacteria in multidrug-resistant biofilms in diabetic wound infections, Adv. Healthcare Mater. 14 (2025) 2405190, https://doi.org/10.1002/adhm.202405190.
[58] X. Han, B. Liang, X. Li, T. Gao, Y. Zhao, W. Zhu, F. Chen, Shape-controlled microneedles for transdermal drug delivery by direct-material-extrusion 3D printing, Virtual, Phys. Prototy. 21 (2026) e2605395, 1080/17452759.2025.2605395.
[59] Y. Han, X. Qin, W. Lin, C. Wang, X. Yin, J. Wu, Y. Chen, X. Chen, T. Chen, Microneedle-based approaches for skin disease treatment, Nano-Micro Lett. 17 (2025) 1–38, https://doi.org/10.1007/s40820-025-01662-y.
[60] Z. Jiang, W. Wu, T. Chen, W. Hu, X. Zhang, C. Zhou, A. Lu, Y. Yan, G. Quan, C. Wu, Barrier-disrupting microneedle technology: overcoming physical, physiological, and pathological skin defenses to enhance therapeutic efficacy, Bioact. Mater. 57 (2026) 400–429, https://doi.org/10.1016/j.bioactmat.2025.11.005.
[61] F. Xie, M. Wang, Q. Chen, T. Chi, S. Zhu, P. Wei, Y. Yang, L. Zhang, X. Li, Z. Liao, Endogenous stimuli-responsive nanoparticles for cancer therapy: from bench to bedside, Pharmacol. Res. 186 (2022) 106522, https://doi.org/10.1016/j.phrs.2022.106522.
[62] J. Yang, A. des Rieux, A. Malfanti, Stimuli-responsive nanomedicines for the treatment of non-cancer related inflammatory diseases, ACS Nano 19 (2025) 15189–15219, https://doi.org/10.1021/acsnano.5c00700.

[63] Z. Liu, J. Chen, M. Xu, S. Ho, Y. Wei, H.-P. Ho, K.-T. Yong, Engineered multi-domain lipid nanoparticles for targeted delivery, Chem. Soc. Rev. 54 (2025) 5961–5994, https://doi.org/10.1039/d4cs00891j.
[64] E.V.A. Otu, S. Rozhkov, G. Sosa, P. Mallikaratchy, Aptamers as target-specific recognition elements in drug delivery, Adv. Drug Deliv. Rev. 226 (2025) 115685, https://doi.org/10.1016/j.addr.2025.115685.
[65] Y. Chen, X. Feng, Gold nanoparticles for skin drug delivery, Int. J. Pharm. 625 (2022) 122122, https://doi.org/10.1016/j.ijpharm.2022.122122.
[66] X. Sun, Q. Wang, H. Bao, Y. Liu, S. Yao, M. Li, N. Chen, Y. Chen, Porphyrinic metal–organic framework PCN-224 nanoparticles for colocalization of nanoparticle-cargo in the skin and enhancement of sonodynamic efficacy, ACS Appl. Nano Mater. 7 (2024) 2614–2629, https://doi.org/10.1021/acsanm.3c04675.
[67] Q. Wang, M. Li, X. Sun, N. Chen, S. Yao, X. Feng, Y. Chen, ZIF-8 integrated with polydopamine coating as a novel nano-platform for skin-specific drug delivery, J. Mater. Chem. B 11 (2023) 1782–1797, https://doi.org/10.1039/d2tb02361j.
[68] M. Rahmati, E.A. Silva, J.E. Reseland, C.A. Heyward, H.J. Haugen, Biological responses to physicochemical properties of biomaterial surface, Chem. Soc. Rev. 49 (2020) 5178–5224, https://doi.org/10.1039/d0cs00103a.
[69] S.T. Moore, X. Lian, A. Vaidya, S. Chatterjee, J. Santelli, Y. Sun, L. Farbiak, H. Zhu, D.J. Siegwart, Multiplexed lipid nanoparticle barcoding reveals tissue-dynamic kinetic insights and enriched cellular tropism in hepatic zones, Nat. Commun. (2026), https://doi.org/10.1038/s41467-025-68103-7.
[70] L. Bai, J. Su, Artificial intelligence virtual organoids (AIVOs), Bioact. Mater. 59 (2026) 45–68, https://doi.org/10.1016/j.bioactmat.2025.12.030.
[71] X. Fu, Z. Sun, J. Gu, R. Liu, M. Ma, X. Ma, Y.-P. Ho, X. Zhang, Y. Zhang, 3D-printed barbed microneedle electrodes for biosensing and drug delivery in wound management, Microsyst. Nanoeng. 12 (2026) 5, https://doi.org/10.1038/s41378-025-01136-6.
[72] J. Han, Z. Wu, S. Zhan, T. Sheng, J. You, J. Yu, J. Fu, Y. Zhang, Z. Gu, Biorhythm-mimicking growth hormone patch, Nat. Mater. 24 (2025) 1–12, https://doi.org/10.1038/s41563-025-02188-9.
[73] Y. Wan, L.H. Fu, C. Li, J. Lin, P. Huang, Conquering the hypoxia limitation for photodynamic therapy, Adv. Mater. 33 (2021) 2103978, https://doi.org/10.1002/adma.202103978.
[74] Y. He, Q. Chang, F. Lu, Oxygen-releasing biomaterials for chronic wounds breathing: from theoretical mechanism to application prospect, Mater. Today Bio 20 (2023) 100687, https://doi.org/10.1016/j.mtbio.2023.100687.
[75] N. Chettouh-Hammas, C. Grillon, Physiological skin oxygen levels: an important criterion for skin cell functionality and therapeutic approaches, Free Radic. Biol. Med. 222 (2024) 259–274, https://doi.org/10.1016/j.freeradbiomed.2024.06.015.
[76] S.M. Evans, A.E. Schrlau, A.A. Chalian, P. Zhang, C.J. Koch, Oxygen levels in normal and previously irradiated human skin as assessed by EF5 binding, J. Invest. Dermatol. 126 (2006) 2596–2606, https://doi.org/10.1038/sj.jid.5700451.
[77] W. Zai, Y. Yuan, L. Kang, J. Xu, Y. Hu, L. Kang, J. Wu, Oxygen penetration through full-thickness skin by oxygen-releasing sutures for skin graft transplantation, Engineering (2023) 29, https://doi.org/10.1016/j.eng.2023.05.006.
[78] M. Stücker, A. Struk, P. Altmeyer, M. Herde, H. Baumgärtl, D.W. Lübbers, The cutaneous uptake of atmospheric oxygen contributes significantly to the oxygen supply of human dermis and epidermis, J. Physiol. 538 (2002) 985–994, https://doi.org/10.1113/jphysiol.2001.013067.
[79] H.R. Rezvani, N. Ali, L.J. Nissen, G. Harfouche, H. De Verneuil, A. Taïeb, F. Mazurier, HIF-1α in epidermis: oxygen sensing, cutaneous angiogenesis, cancer, and non-cancer disorders, J. Invest. Dermatol. 131 (2011) 1793–1805, https://doi.org/10.1038/jid.2011.141.
[80] K. Nys, H. Maes, A.M. Dudek, P. Agostinis, Uncovering the role of hypoxia inducible factor-1α in skin carcinogenesis, Biochim. Biophys. Acta 1816 (2011) 1–12, https://doi.org/10.1016/j.bbcan.2011.02.001.
[81] T. Hagen, Oxygen versus reactive oxygen in the regulation of HIF-1α: the balance tips, Biochem. Res. Int. 2012 (2012) 436981, https://doi.org/10.1155/2012/436981.
[82] S. Yao, F. Xu, Y. Wang, J. Shang, S. Li, X. Xu, Z. Liu, W. He, Z. Guo, Y. Chen, Photoinduced synergism of ferroptosis/pyroptosis/oncosis by an O_2-independent photocatalyst for enhanced tumor immunotherapy, J. Am. Chem. Soc. 147 (2025) 11132–11144, https://doi.org/10.1021/jacs.4c17268.
[83] L. Ge, C. Qiao, Y. Tang, X. Zhang, X. Jiang, Light-activated hypoxia-sensitive covalent organic framework for tandem-responsive drug delivery, Nano Lett. 21 (2021) 3218–3224, https://doi.org/10.1021/acs.nanolett.1c00488.
[84] P.-W. Chen, Y.-M. Zhang, L.-S. Li, B.-B. Liu, L. Chen, X. Yang, M.-X. Zhao, A hypoxia-activated nano prodrug for enhanced chemotherapy and photodynamic synergistic therapy with minimized chemotherapy side effect, Mater. Today Chem. 48 (2025) 102932, https://doi.org/10.1016/j.mtchem.2025.102932.
[85] P.Z. Liang, L.L. Ren, Y.H. Yan, Z. Li, F.Y. Yang, T.B. Ren, L. Yuan, X.B. Zhang, Activatable photosensitizer prodrug for self-amplified immune therapy via pyroptosis, Angew Chem. Int. Ed. Engl. 137 (2025) e202419376, https://doi.org/10.1002/anie.202419376.
[86] J. Yu, J. Wu, J. Huang, C. Xu, M. Xu, C.Z.H. Koh, K. Pu, Y. Zhang, Hypoxia-tolerant polymeric photosensitizer prodrug for cancer photo-immunotherapy, Nat. Commun. 16 (1) (2025) 153, https://doi.org/10.1038/s41467-024-55529-8.
[87] S. Qin, Y. Xu, H. Li, H. Chen, Z. Yuan, Recent advances in in situ oxygen-generating and oxygen-replenishing strategies for hypoxic-enhanced photodynamic therapy, Biomater. Sci. 10 (2022) 51–84, https://doi.org/10.1039/d1bm00317h.
[88] A.R. Hernández, M. Boutonnet, B. Svensson, E. Butler, R. Lood, K. Blom, B. Vallejo, C. Anderson, J. Engblom, T. Ruzgas, New concepts for transdermal delivery of oxygen based on catalase biochemical reactions studied by oxygen electrode amperometry, J. Contr. Release 306 (2019) 121–129, https://doi.org/10.1016/j.jconrel.2019.06.001.
[89] S. Nocchi, S. Björklund, B. Svensson, J. Engblom, T. Ruzgas, Electrochemical monitoring of native catalase activity in skin using skin covered oxygen electrode, Biosens. Bioelectron. 93 (2017) 9–13, https://doi.org/10.1016/j.bios.2017.01.001.
[90] G.-e. Rhie, J.Y. Seo, J.H. Chung, Modulation of catalase in human skin in vivo by acute and chronic UV radiation, Mol. Cells 11 (2001) 399–404, https://doi.org/10.1016/S1016-8478(23)17053-1.
[91] N.G. Gavalas, S. Akhtar, D.J. Gawkrodger, P.F. Watson, A.P. Weetman, E. H. Kemp, Analysis of allelic variants in the catalase gene in patients with the skin depigmenting disorder vitiligo, Biochem. Biophys. Res. Commun. 345 (2006) 1586–1591, https://doi.org/10.1016/j.bbrc.2006.05.063.
[92] H. Wang, Y. Xie, Y. Chen, H. Zhao, X. Lv, Z. Zhang, G. Li, J. Pan, J. Wang, Z. Liu, Transdermal delivery of photosensitizer-catalase conjugate by fluorinated polyethylenimine for enhanced topical photodynamic therapy of bacterial infections, Adv. Healthcare Mater. 12 (2023) 2300848, https://doi.org/10.1002/adhm.202300848.
[93] Y. Li, G. He, L.-H. Fu, M.R. Younis, T. He, Y. Chen, J. Lin, Z. Li, P. Huang, A microneedle patch with self-oxygenation and glutathione depletion for repeatable photodynamic therapy, ACS Nano 16 (2022) 17298–17312, https://doi.org/10.1021/acsnano.2c08098.
[94] K. Thakur, C. Attri, A. Seth, Nanocarriers-based immobilization of enzymes for industrial application, 3 Biotech 11 (2021) 427, https://doi.org/10.1007/s13205-021-02953-y.
[95] S. Cao, P. Xu, Y. Ma, X. Yao, Y. Yao, M. Zong, X. Li, W. Lou, Recent advances in immobilized enzymes on nanocarriers, Chinese, J. Catal. 37 (2016) 1814–1823, https://doi.org/10.1016/S1872-2067(16)62528-7.
[96] J.H. Santos, C.A. Oliveira, B.M. Rocha, G. Carretero, C.O. Rangel-Yagui, Pegylated catalase as a potential alternative to treat vitiligo and UV induced skin damage, Bioorg. Med. Chem. 30 (2021) 115933, https://doi.org/10.1016/j.bmc.2020.115933.
[97] M. Bilal, N. Khaliq, M. Ashraf, N. Hussain, Z. Baqar, J. Zdarta, T. Jesionowski, H. M. Iqbal, Enzyme mimic nanomaterials as nanozymes with catalytic attributes, Colloids Surf., B 221 (2023) 112950, https://doi.org/10.1016/j.colsurfb.2022.112950.
[98] C.-M. Lai, X.-S. Xiao, J.-Y. Chen, W.-Y. He, S.-S. Wang, Y. Qin, S.-H. He, Revolutionizing nanozymes: the synthesis, enzyme-mimicking capabilities of carbon dots, and advancements in catalytic mechanisms, Int. J. Biol. Macromol. 293 (2025) 139284, https://doi.org/10.1016/j.ijbiomac.2024.139284.
[99] M. Kajita, K. Hikosaka, M. Iitsuka, A. Kanayama, N. Toshima, Y. Miyamoto, Platinum nanoparticle is a useful scavenger of superoxide anion and hydrogen peroxide, free, Radic. Res. 41 (2007) 615–626, https://doi.org/10.1080/10715760601169679.
[100] D. Xu, L. Wu, H. Yao, L. Zhao, Catalase-like nanozymes: classification, catalytic mechanisms, and their applications, Small 18 (2022) 2203400, https://doi.org/10.1002/smll.202203400.
[101] M. Tang, Z. Zhang, T. Sun, B. Li, Z. Wu, Manganese-based nanozymes: preparation, catalytic mechanisms, and biomedical applications, Adv. Healthcare Mater. 11 (2022) 2201733, https://doi.org/10.1002/adhm.202201733.
[102] C. Wang, Y. Xiao, W. Zhu, J. Chu, J. Xu, H. Zhao, F. Shen, R. Peng, Z. Liu, Photosensitizer-modified MnO2 nanoparticles to enhance photodynamic treatment of abscesses and boost immune protection for treated mice, Small 16 (2020) 2000589, https://doi.org/10.1002/smll.202000589.
[103] K. Wu, H. Zhao, Z. Sun, B. Wang, X. Tang, Y. Dai, M. Li, Q. Shen, H. Zhang, Q. Fan, Endogenous oxygen generating multifunctional theranostic nanoplatform for enhanced photodynamic-photothermal therapy and multimodal imaging, Theranostics 9 (2019) 7697, https://doi.org/10.7150/thno.38565.
[104] J. Li, Z. Chu, S. Wang, H. Liu, B. Dong, Study on synergistic mechanism of Cu-TCPP@ MnO2 composites for photothermal/photodynamic/chemodynamic treatment of infected wound healing, Chem. Eng. J. 512 (2025) 162334, https://doi.org/10.1016/j.cej.2025.162334.
[105] H. He, M. Long, Y. Duan, N. Gu, Prussian blue nanozymes: progress, challenges, and opportunities, Nanoscale 15 (2023) 12818–12839, https://doi.org/10.1039/d3nr01741a.
[106] W. Zhang, S. Hu, J.-J. Yin, W. He, W. Lu, M. Ma, N. Gu, Y. Zhang, Prussian blue nanoparticles as multienzyme mimetics and reactive oxygen species scavengers, J. Am. Chem. Soc. 138 (2016) 5860–5865, https://doi.org/10.1021/jacs.5b12070.
[107] K. Feng, Z. Wang, S. Wang, G. Wang, H. Dong, H. He, H. Wu, M. Ma, X. Gao, Y. Zhang, Elucidating the catalytic mechanism of Prussian blue nanozymes with self-increasing catalytic activity, Nat. Commun. 15 (2024) 5908, https://doi.org/10.1038/s41467-024-50344-7.
[108] A. Tong, C. Tong, J. Fan, J. Shen, C. Yin, Z. Wu, J. Zhang, B. Liu, Prussian blue nano-enzyme-assisted photodynamic therapy effectively eradicates MRSA infection in diabetic mouse skin wounds, Biomater. Sci. 11 (2023) 6342–6356, https://doi.org/10.1039/d3bm01039b.
[109] N. Mohanto, H. Mondal, Y.-J. Park, J.-P. Jee, Therapeutic delivery of oxygen using artificial oxygen carriers demonstrates the possibility of treating a wide range of diseases, J. Nanobiotechnol. 23 (2025) 25, https://doi.org/10.1186/s12951-024-03060-9.

[110] Z. Wang, T. Chen, X. Li, B. Guo, P. Liu, Z. Zhu, R.X. Xu, Oxygen-releasing biomaterials for regenerative medicine, J. Mater. Chem. B 11 (2023) 7300–7320, https://doi.org/10.1039/d3tb00670k.
[111] X. Zhang, G. Chen, Y. Liu, L. Sun, L. Sun, Y. Zhao, Black phosphorus-loaded separable microneedles as responsive oxygen delivery carriers for wound healing, ACS Nano 14 (2020) 5901–5908, https://doi.org/10.1021/acsnano.0c01059.
[112] P. Liu, Y. Fu, F. Wei, T. Ma, J. Ren, Z. Xie, S. Wang, J. Zhu, L. Zhang, J. Tao, Microneedle patches with O2 propellant for deeply and fast delivering photosensitizers: towards improved photodynamic therapy, Adv. Sci. 9 (2022) 2202591, https://doi.org/10.1002/advs.202202591.
[113] Z. Zhu, L. Wang, Y. Peng, X. Chu, L. Zhou, Y. Jin, H. Guo, Q. Gao, J. Yang, X. Wang, Continuous self-oxygenated double-layered hydrogel under natural light for real-time infection monitoring, enhanced photodynamic therapy, and hypoxia relief in refractory diabetic wounds healing, Adv. Funct. Mater. 32 (2022) 2201875, https://doi.org/10.1002/adfm.202201875.
[114] S. Zhang, N. Yang, S. Sun, H. Zhao, W. Wang, J. Nie, Z. Pei, W. He, L. Zhang, L. Cheng, Dually fluorinated unimolecular micelles for stable oxygen-carrying and enhanced photosensitive efficiency to boost photodynamic therapy against hypoxic tumors, Acta Biomater. 193 (2025) 406–416, https://doi.org/10.1016/j.actbio.2025.01.017.
[115] J. Jägers, A. Wrobeln, K.B. Ferenz, Perfluorocarbon-based oxygen carriers: from physics to physiology, Pflügers Archiv 473 (2021) 139–150, https://doi.org/10.1007/s00424-020-02482-2.
[116] P.J. Park, H. Mondal, B.S. Pi, S.T. Kim, J.-P. Jee, The effect of oxygen supply using perfluorocarbon-based nanoemulsions on human hair growth, J. Mater. Chem. B 12 (2024) 991–1000, https://doi.org/10.1039/d3tb02237d.
[117] P.S. Patil, N. Fountas-Davis, H. Huang, M.M. Evancho-Chapman, J.A. Fulton, L. P. Shriver, N.D. Leipzig, Fluorinated methacrylamide chitosan hydrogels enhance collagen synthesis in wound healing through increased oxygen availability, Acta Biomater. 36 (2016) 164–174, https://doi.org/10.1016/j.actbio.2016.03.022.
[118] S. Akula, I.K. Brosch, N.D. Leipzig, Fluorinated methacrylamide chitosan hydrogels enhance cellular wound healing processes, Ann. Biomed. Eng. 45 (2017) 2693–2702, https://doi.org/10.1007/s10439-017-1893-6.
[119] A. Wijekoon, N. Fountas-Davis, N.D. Leipzig, Fluorinated methacrylamide chitosan hydrogel systems as adaptable oxygen carriers for wound healing, Acta, Biomaterials 9 (2013) 5653–5664, https://doi.org/10.1016/j.actbio.2012.10.034.
[120] K.-H. Hsiao, C.-M. Huang, Y.-H. Lee, Development of rifampicin-indocyanine green-loaded perfluorocarbon nanodroplets for photo-chemo-probiotic antimicrobial therapy, Front. Pharmacol. 9 (2018) 1254, https://doi.org/10.3389/fphar.2018.01254.
[121] S. Tian, S. Tan, M. Fan, W. Gong, T. Yang, F. Jiao, H. Qiao, Hypoxic environment of wounds and photosynthesis-based oxygen therapy, Burns. Trauma. 12 (2024), https://doi.org/10.1093/burnst/tkae012 tkae012.
[122] C. Yin, Z. Wang, C. Dai, B. Yang, W. Wang, E. Yang, F. Guo, C. Fan, P. Zhang, J. Sun, Light-triggered photosynthetic engineered bacteria for enhanced-photodynamic therapy by relieving tumor hypoxic microenvironment, Theranostics 13 (5) (2023) 1632, https://doi.org/10.7150/thno.81718.
[123] J. Wang, H. Li, Q. Su, J. Liu, K. Li, Z. Wang, L. Wang, Living photosynthetic micro/nano-platforms: engineering unicellular algae for biomedical applications, Bioact. Mater. 51 (2025) 575–597, https://doi.org/10.1016/j.bioactmat.2025.05.023.
[124] Y. Zhang, H. Liu, X. Dai, H. Li, X. Zhou, S. Chen, J. Zhang, X.-J. Liang, Z. Li, Cyanobacteria-based near-infrared light-excited self-supplying oxygen system for enhanced photodynamic therapy of hypoxic tumors, Nano Res. 14 (2021) 667–673, https://doi.org/10.1007/s12274-020-3094-0.
[125] Z. Liu, L. Lei, Z. Zhang, M. Du, Z. Chen, Ultrasound-responsive engineered bacteria mediated specific controlled expression of catalase and efficient radiotherapy, Mater. Today Bio 31 (2025) 101620, https://doi.org/10.1016/j.mtbio.2025.101620.
[126] N. Labecka, M. Szczepanczyk, E. Mojumdar, E. Sparr, S. Björklund, Unraveling UVB effects: catalase activity and molecular alterations in the stratum corneum, J. Colloid Interface Sci. 666 (2024) 176–188, https://doi.org/10.1016/j.jcis.2024.03.200.
[127] X. Ren, D. Chen, Y. Wang, H. Li, Y. Zhang, H. Chen, X. Li, M. Huo, Nanozymes-recent development and biomedical applications, J. Nanobiotechnol. 20 (1) (2022) 92, https://doi.org/10.1186/s12951-022-01295-y.
[128] C. Zhu, C. Jiang, H.K. Lee, Y. Zhang, S. Tang, All nanozyme-based cascade reactions for biomedical applications: from self-cascading nanozyme to immobilized cascade nanozyme, Adv. Sci. (2025) e19656, https://doi.org/10.1002/advs.202519656.
[129] L. Liu, K. Hou, S. Lin, Y. Di, Z. Zhuang, Z. Zeng, Y. Sun, C. Ji, C. Huang, R. Xiong, Hemoglobin based oxygen carrier and its application in biomedicine, Coord. Chem. Rev. 532 (2025) 216508, https://doi.org/10.1016/j.ccr.2025.216508.
[130] T. Zhang, D. Liu, Y. Zhang, L. Chen, W. Zhang, T. Sun, Biomedical engineering utilizing living photosynthetic Cyanobacteria and microalgae: current status and future prospects, Mater. Today Bio 27 (2024) 101154, https://doi.org/10.1016/j.mtbio.2024.101154.
[131] J. Liu, Y. Li, D. Wang, X. Liu, D. Sun, Y. Wang, Y. Zhang, H. Wang, Engineered cyanobacteria-based self-supplying photosensitizer nano-biosystem for photodynamic therapy, Chem. Eng. J. 495 (2024) 153656, 0.1016/j.cej.2024.153656.
[132] A. Urazaliyeva, P. Kanabekova, A. Beisenbayev, G. Kulsharova, T. Atabaev, S. Kim, C.-K. Lim, All organic nanomedicine for PDT-PTT combination therapy of cancer cells in hypoxia, Sci. Rep. 14 (2024) 17507, https://doi.org/10.1038/s41598-024-68077-4.
[133] F. Sozmen, M. Kucukoflaz, M. Ergul, Z.D.S. Inan, Nanoparticles with PDT and PTT synergistic properties working with dual NIR-light source simultaneously, RSC Adv. 11 (2021) 2383–2389, https://doi.org/10.1039/D0RA09954F.
[134] L. Finlayson, I.R. Barnard, L. McMillan, S.H. Ibbotson, C.T.A. Brown, E. Eadie, K. Wood, Depth penetration of light into skin as a function of wavelength from 200 to 1000 nm, Photochem. Photobiol. 98 (2022) 974–981, https://doi.org/10.1111/php.13550.
[135] T. Yu, J. Zhu, D. Li, D. Zhu, Physical and chemical mechanisms of tissue optical clearing, iScience 24 (2021), https://doi.org/10.1016/j.isci.2021.102178.
[136] Q. Xia, D. Li, T. Yu, J. Zhu, D. Zhu, In vivo skin optical clearing for improving imaging and light-induced therapy: a review, J. Biomed. Opt. 28 (2023), https://doi.org/10.1117/1.JBO.28.6.060901, 060901-060901.
[137] A. Liopo, R. Su, D.A. Tsyboulski, A.A. Oraevsky, Optical clearing of skin enhanced with hyaluronic acid for increased contrast of optoacoustic imaging, J. Biomed. Opt. 21 (2016), https://doi.org/10.1117/1.JBO.21.8.081208, 081208-081208.
[138] Y. Liu, D. Zhu, J. Xu, Y. Wang, W. Feng, D. Chen, Y. Li, H. Liu, X. Guo, H. Qiu, Penetration-enhanced optical coherence tomography angiography with optical clearing agent for clinical evaluation of human skin, Photodiagnosis Photodyn. Ther. 30 (2020) 101734, https://doi.org/10.1016/j.pdpdt.2020.101734.
[139] Y. Chu, W. Zhang, B. Yuan, X.-Q. Xu, Y. Ma, Y. Wang, Deepened photodynamic therapy through skin optical clearing technology in the visible light Window, Langmuir 40 (2023) 1007–1015, https://doi.org/10.1021/acs.langmuir.3c03231.
[140] M. Ouyang, X. Wang, Y. Fu, G. Xie, S. Du, Y. Li, L. Zhang, J. Tao, J. Zhu, Skin optical clearing enabled by dissolving hyaluronic acid microneedle patches, Int. J. Biol. Macromol. 220 (2022) 1188–1196, https://doi.org/10.1016/j.ijbiomac.2022.08.153.
[141] S. Coppola, V. Vespini, G. Nasti, P. Ferraro, Transmitting light through biocompatible and biodegradable drug delivery micro needles, Ieee. J. Sel. Top. Quant. 27 (2021) 1–8, https://doi.org/10.1109/JSTQE.2021.3057834.
[142] S. Charoensuksira, S. Rattanapirat, J. Meephansan, P. Sirithanabadeekul, P. Adulyaritthikul, S. Thongma, Y. Rayanasukha, K. Tantisantisom, The efficacy of light-guiding microneedle patch for stimulating hair growth in androgenetic alopecia, Arch. Dermatol. Res. 316 (2024) 639, https://doi.org/10.1007/s00403-024-03396-0.
[143] Z.Q. Zhao, S.L. Zhang, R. Yu, Z.Y. Wang, X. Sun, Z.W. Zhang, X.Y. Geng, L. Liang, Y. Cui, B.Z. Chen, Optical microneedle-enhanced transdermal light scattering for in situ photothermal therapy targeting basal-layer psoriasis, ACS Appl. Mater. Interfaces 17 (2025) 19446–19458, https://doi.org/10.1021/acsami.4c23014.
[144] H. Zhao, X. Wang, J. Xiong, G. Liang, X. Wu, J. Xi, Y. Zhang, Z. Li, X. Hu, Z. Wei, Miniaturized all-in-one microneedle device for point of care light therapy, Npj. Flex. Electron. 8 (2024) 32, https://doi.org/10.1038/s41528-024-00317-z.
[145] M. Oungeun, S. Wanichwecharungruang, E. Miyako, Wireless light-emitting diode-driven functional microneedle devices for skin cancer therapy, Adv. Ther. 7 (2024) 2400233, https://doi.org/10.1002/adtp.202400233.
[146] J. Liu, B. Sun, W. Li, H.-J. Kim, S.U. Gan, J.S. Ho, J.N.B. Rahmat, Y. Zhang, Wireless sequential dual light delivery for programmed PDT in vivo, Light, Sci. Appl. 13 (2024) 113, https://doi.org/10.1038/s41377-024-01437-x.
[147] S. Zhang, C. Qu, Y. Xiao, H. Liu, G. Song, Y. Xu, Flexible alternating current electroluminescent devices integrated with high voltage triboelectric nanogenerators, Nanoscale 14 (2022) 4244–4253, https://doi.org/10.1039/d1nr08203e.
[148] J. Zhang, X. Mao, Q. Jia, R. Nie, Y. Gao, K. Tao, H. Chang, P. Li, W. Huang, Body-worn and self-powered flexible optoelectronic device for metronomic photodynamic therapy, Npj. Flex. Electron. 8 (2024) 60, https://doi.org/10.1038/s41528-024-00345-9.
[149] M. Overchuk, R. Weersink, B. Wilson, G. Zheng, Photodynamic and photothermal therapies: synergy opportunities for nanomedicine, ACS Nano 17 (2023) 7979–8003, https://doi.org/10.1021/acsnano.3c00891.
[150] K. Choudhary, N.K. Dhania, Light-activated nanoweapons: aPDT and PTT strategies against persistent infections and biofilms, J. Drug Deliv. Sci. Technol. 115 (2025) 107676, https://doi.org/10.1016/j.jddst.2025.107676.
[151] L. Fang, Z. Chen, J. Dai, Y. Pan, Y. Tu, Q. Meng, Y. Diao, S. Yang, W. Guo, L. Li, Recent advances in strategies to enhance photodynamic and photothermal therapy performance of single-component organic phototherapeutic agents, Adv. Sci. 12 (2025) 2409157, https://doi.org/10.1002/advs.202409157.
[152] Z. Li, X. Lai, S. Fu, L. Ren, H. Cai, H. Zhang, Z. Gu, X. Ma, K. Luo, Immunogenic cell death activates the tumor immune microenvironment to boost the immunotherapy efficiency, Adv. Sci. 9 (2022) 2201734, https://doi.org/10.1002/advs.202201734.
[153] Z. Xie, M. Peng, R. Lu, X. Meng, W. Liang, Z. Li, M. Qiu, B. Zhang, G. Nie, N. Xie, Black phosphorus-based photothermal therapy with aCD47-mediated immune checkpoint blockade for enhanced cancer immunotherapy, Light, Sci. Appl. 9 (2020) 161, https://doi.org/10.1038/s41377-020-00388-3.
[154] Z. Xie, Y. Duo, T. Fan, Y. Zhu, S. Feng, C. Li, H. Guo, Y. Ge, S. Ahmed, W. Huang, Light-induced tumor theranostics based on chemical-exfoliated borophene, Light Sci. Appl. 11 (2022) 324, https://doi.org/10.1038/s41377-022-00980-9.
[155] L. Chen, J. Huang, L. Liu, M. Tong, X. He, S. Zhao, Q. Diao, H. Chen, J. Zeng, M. Lan, Multimodal cascade-amplified phototheranostics for enhanced anti-tumor immunity, Biomaterials 325 (2026) 123634, https://doi.org/10.1016/j.biomaterials.2025.123634.
[156] Y. Zhao, X. Liu, X. Liu, J. Yu, X. Bai, X. Wu, X. Guo, Z. Liu, X. Liu, Combination of phototherapy with immune checkpoint blockade: theory and practice in cancer, Front. Immunol. 13 (2022) 955920, https://doi.org/10.3389/fimmu.2022.955920.

[157] X. Yu, Y. Zhang, Z. Rong, X. Li, L. Luo, L. Zhang, L. Sun, Y. Liu, W. Li, L. Mei, Engineering NK cell membrane-camouflaged copper-BODIPY nanoassembly to synergize dual-phototherapy and cuproptosis for enhanced antitumor immunity, Chem. Eng. J. 526 (2025) 170867, https://doi.org/10.1016/j.cej.2025.170867.
[158] Z. Kejík, J. Hajduch, N. Abramenko, F. Vellieux, K. Veselá, J.L. Fialová, K. Petrláková, K. Kučnirová, R. Kaplánek, A. Tatar, Cyanine dyes in the mitochondria-targeting photodynamic and photothermal therapy, Commun. Chem. 7 (2024) 180, https://doi.org/10.1038/s42004-024-01256-6.
[159] S. Li, S. Wang, Y. Cai, D. Hua, J. Jin, H. Zhang, Z. Yang, Purpurin/Indocyanine green nanocomposite for restricting glutaminolysis to enhance dual phototherapy of cancer, Mol. Pharm. 22 (2025) 3073–3083, https://doi.org/10.1021/acs.molpharmaceut.5c00001.
[160] W.-L. Xia, X.-Y. Ran, K.-P. Xie, Y. Zhao, J. Chen, Q. Zhou, X.-Q. Yu, K. Li, Optimized indocyanine green nanopreparations for biomedical applications, Coord. Chem. Rev. 528 (2025) 216422, https://doi.org/10.1016/j.ccr.2024.216422.
[161] T. Zhu, Z. Sang, Z. Ye, X. Guo, X. Qu, Y. Hao, W. Wang, Local delivery of celecoxib/indocyanine green-loaded nanomodulators for combinational photothermal/photodynamic/anti-cyclooxygenase-2 therapy of oral leukoplakia, Chem. Eng. J. 505 (2025) 159734, 0.1016/j.cej.2025.159734.
[162] Z. Yu, X. Meng, S. Zhang, X. Wang, Y. Chen, P. Min, Z. Zhang, Y. Zhang, IR-808 loaded nanoethosomes for aggregation-enhanced synergistic transdermal photodynamic/photothermal treatment of hypertrophic scars, Biomater. Sci. 10 (2022) 158–166, https://doi.org/10.1039/d1bm01555a.
[163] X. Yang, D. Wang, J. Zhu, L. Xue, C. Ou, W. Wang, M. Lu, X. Song, X. Dong, Functional black phosphorus nanosheets for mitochondria-targeting photothermal/photodynamic synergistic cancer therapy, Chem. Sci. 10 (2019) 3779–3785, https://doi.org/10.1039/c8sc04844d.
[164] C. Wu, D. Li, L. Wang, X. Guan, Y. Tian, H. Yang, S. Li, Y. Liu, Single wavelength light-mediated, synergistic bimodal cancer photoablation and amplified photothermal performance by graphene/gold nanostar/photosensitizer theranostics, Acta Biomater. 53 (2017) 631–642, https://doi.org/10.1016/j.actbio.2017.01.078.
[165] E. Celikbas, A. Saymaz, H. Gunduz, I. Koc, E. Cakir, A. Sennaroglu, S. Kolemen, H. Yagci Acar, K. Onbasli, Image-guided enhanced PDT/PTT combination therapy using brominated hemicyanine-loaded folate receptor-targeting Ag2S quantum dots, Bioconjug. Chem. 34 (2023) 880–892, https://doi.org/10.1021/acs.bioconjchem.3c00096.
[166] W. Fu, Q. Lu, S. Xing, L. Yan, X. Zhang, Iron-doped metal-zinc-centered organic framework mesoporous carbon derivatives for single-wavelength nir-activated photothermal/photodynamic synergistic therapy, Langmuir 39 (2023) 6505–6513, https://doi.org/10.1021/acs.langmuir.3c00430.
[167] T. Yu, X. Zhong, D. Li, J. Zhu, V.V. Tuchin, D. Zhu, Delivery and kinetics of immersion optical clearing agents in tissues: optical imaging from ex vivo to in vivo, Adv. Drug Deliv. Rev. 215 (2024) 115470, https://doi.org/10.1016/j.addr.2024.115470.
[168] S.-H. Jeong, M.-G. Lee, C.-C. Kim, J. Park, Y. Baek, B.I. Park, J. Doh, J.-Y. Sun, An implantable ionic therapeutic platform for photodynamic therapy with wireless capacitive power transfer, Mater. Horiz. 10 (2023) 2215–2225, https://doi.org/10.1039/d2mh01548j.
[169] L. Zhang, Y. Zhu, R. Zhang, W.-J. Wang, H. Yang, H. Tan, Y. Xiong, B.Z. Tang, Z. Zhao, Tumor microenvironment-responsive nanoshield for precision photodynamic and photothermal synergistic cancer therapy with mitigated skin phototoxicity, Biomaterials 327 (2026) 123740, https://doi.org/10.1016/j.biomaterials.2025.123740.
[170] M. Lin, X. Kang, F. Liu, J.J. Nie, J. Zhang, J. Zhuang, B. Yu, F.J. Xu, Implantable light source-integrated microneedles for losartan-enhanced and sustained photodynamic therapy of tumors, Adv. Funct. Mater. (2025) e13208, https://doi.org/10.1002/adfm.202513208.
[171] R. Nie, Q. Jia, Y. Li, C. Yan, X. Liu, Y. Tao, J. Zhang, P. Li, W. Huang, Implantable biophotonic device for wirelessly cancer real-time monitoring and modulable treatment, Adv. Sci. 12 (2025) 2503778, https://doi.org/10.1002/advs.202503778.
[172] N. Kwon, H. Weng, M.A. Rajora, G. Zheng, Activatable photosensitizers: from fundamental principles to advanced designs, Angew. Chem., Int. Ed. Engl. 64 (2025) e202423348, https://doi.org/10.1002/anie.202423348.